PARAPET

Evaluation of iterative algorithms

Document : D/5.6/

HAMMERSMITH/THIELEMANS-SPINKS
MILAN/BETTINARDI-PAGANI-GILARDI
TECHNION/JACOBSON-MARGALIT-GORDON-LEFKOVITZ-BEN-TAL
BRUNEL/SADKI-MITRA
GENEVA/LABBE-MOREL
                    /16-Jul-04/1/1.0

COMPLETE DELIVERABLE

Approved by:

K. Thielemans	V. Friedrich
(Author)	(Project manager)

1. Introduction

The evaluation of different iterative algorithms described in this document is mainly based on data from test objects (phantoms) that provide information on the fundamental parameters of contrast recovery and signal-to-noise ratio. These phantoms are chosen (a) to give precise geometrical configurations and/or (b) to simulate the distribution of structures in the brain and chest/abdomen with known contrast ratios. Although some clinical studies are analysed as well, determination of the efficacy of each algorithm with clinical data is a longer-term goal which would require large sets of data and observation by clinical personnel in a "double-blind" format. The phantom data reflects the increasing use of positron tomography for tumour detection but also includes specific anatomical/physiological structures in the brain. Data have also been acquired from a full-ring scanner, used more for research applications and a partial-ring (rotating) scanner more applicable to clinical diagnosis.

The principal comparison has been made between maximum-likelihood type algorithms using a "ordered subsets" (OS) approach, where the image is updated after performing computation on only a subset of the measured data. This accelerates the reconstruction to the desired "stopping criterion" although some methods do not strictly converge in a mathematical sense. The types of algorithm employed are (i) expectation-maximisation (OSEM), (ii) mirror descent (OSMD) and (iii) conjugate barrier (OSCB). In addition, the effects of (a) filtering and (b) use of prior information during the reconstruction process have been tested. The Metz filter is introduced in an attempt to provide smoothing as well as "feature amplification" by matching filter parameters to lesion size. The median root prior (MRP) is introduced as a "penalty function" which imposes local monotonicity in the image. Comparison of the various iterative methods is made with the standard method of filtered backprojection, the PROMIS (or 3DRP) algorithm. Finally, some results are included on Block-ART.

2. Quantitative criteria for comparison

Performance was mainly evaluated quantitatively with respect to two Figures Of Merit (FOMs), namely the coefficient of variation (CV) and contrast recovery (CR), see also **D1.2**. Coefficient of variation is a measure of noise and is defined [NEMA] as the ratio of the standard deviation to the mean of the image over some Region of Interest (ROI).

$$CV = (\textstyle\sum (v_i - m)^2) / N)^{1/2} / m$$

where v_i are the voxel values (voxels lying entirely in the ROI) , m is the mean value for the ROI and N is the number of voxels. CV is positive and should be as small as possible. Contrast recovery measures differences in reconstructed activity levels. Imitating [Dau99], we computed CR between a localised, low-activity (cold) region and a background region as

$$CR_{cold} = 1 - (mean(local)/mean(background)).$$

where mean(local) and mean(background) refer to means taken over appropriately placed ROIs. CR_{cold} should be as high as possible (and close to 1). For locally hot regions, we computed

$$CR_{hot} = (mean(local)/mean(background)) - 1$$

which, although not normalised to the true value, was sufficient for the purposes of algorithm cross-comparison. Our aim is to determine which algorithm provides the best trade-off between contrast and noise control.

3. Maximum-likelihood type algorithms

In this section we discuss the evaluation of three different maximum likelihood type algorithms: Ordered Subsets Expectation Maximisation (OSEM), Ordered Subsets Mirror Descent (OSMD) and Ordered Sets Conjugate Barrier (OSCB). The material from this section is taken from [Mar99]. We first briefly review these algorithms.

The long established Expectation-Maximisation (EM) method [She82, Va85] for maximising the likelihood function has the major drawback that it converges very slowly, requiring many computationally very intensive iterations before reasonable images are obtained. The OSEM algorithm [Hud94] uses an acceleration technique based on the Ordered Sets (OS) idea, where the image is updated after doing an EM step on only a subset of the measured data. The theoretical properties of this algorithm are not very appealing. It is known to converge only under two stringent assumptions: "consistency" of the data, and the subsets being "balanced" (see [Hud94] for details). In particular the first assumption is never satisfied for real PET measurements, as it roughly requires that there is no noise in the data. Nevertheless, in practice it has been shown extensively in the literature that especially during the first iterations, use of the OS technique results in a time saving compared to EM by a factor close to the number of subsets (provided there are not too many subsets). This observation, together with the fact that the EM algorithm is normally stopped early anyway because of a 'deterioration' of the image at high iteration number, has made the OSEM algorithm very popular, and it can be considered as a benchmark against which new methods should be compared.

Both OSMD and OSCB are new algorithms developed within the PARAPET project, see **D5.5**. These algorithms are a type of gradient descent methods, but with the step taken in the dual normed space of the original variables. In contrast to OSEM, the OSMD method [Ben99] and the OSCB method [Ben99b] were shown to converge to the MLE without additional restricting assumptions. More importantly, for these methods an upper bound on the error in the objective function value was obtained, showing that at the N-th iteration the error is proportional to $1/\sqrt{N}$. Moreover, for a problem with n variables, the error bound is proportional to $\sqrt{\log n}$, which means that it is "almost independent" of the problem's dimension. This latter property is particularly meaningful for problems that are of very large scale, as indeed is the case for PET reconstruction.

In spite of the above differences, the computational effort required by the three methods is essentially the same; they all require in each iteration a forward and back projection step, which are by far the major time consuming operations.

Both OSMD and OSCB are non-monotonic, in contrast to EM.[1] That is, the next (sub)iteration is not guaranteed to give higher likelihood.[2] This has some consequences on the evaluation as presented below. In (OS)EM the FOMs have roughly monotonic behaviour in terms of iteration number. This is not always true for OSMD and OSCB.

The performance of the algorithms was evaluated on acquired phantom data from a GE Advance [Gem99] scanner and on simulated phantom and clinical data from the PRT-1 scanner [Tow93]. We measured the performance of OSMD, OSCB and OSEM in terms of noise control, contrast recovery and stability with respect to increasing number of iterations. The OSMD and the OSCB algorithms produce reconstructed images with high quality and compare well with OSEM. The reconstructions are more uniform than those of OSEM, with the expense of only a slight reduction in contrast. In fact, for the clinical data test, OSCB was superior in both figures of merit. In addition, OSMD and OSCB reconstructions remain more stable than OSEM as the number of iterations increases.

---

[1] Also OSEM is not monotonic. However, it tends to be monotonic in the first iterations, depending on the noise in the data.

[2] We did experiment with a modification where for each iteration, we evaluated the image with the highest likelihood instead of just the current estimate. Both visual quality and FOMs followed the same trends as the results presented here.

3.1 Data and procedures

The tests include acquired phantom data from a GE Advance scanner, and simulated phantom data, obtained from the Eidolon simulator ([Zai98], [Zai99], **D2.1**), for the PRT-1 scanner. In addition, we tested a clinical study from the PRT-1 scanner. All projection data, obtained on both the GE Advance and PRT-1 scanners, were pre-corrected for detector efficiency, scatter, randoms and attenuation. The phantoms that we consider for the GE Advance scanner are the *Jaszczak* phantom and the *Whole Body* phantom, and for the PRT-1 scanner, the *Hot Spheres* phantom.

The Hot Spheres phantom is used to test tumour detection capability, mainly for torso studies. It consists of a collection of spherical regions of high radioactivity levels, representing tumours, in a background of low radioactivity. The Jaszczak phantom is used to check resolution, mainly for brain studies. It consists of a radioactive cylinder with non-radioactive cylindrical inserts of different radii. (Resolution is indicated by the number and sizes of inserts that are observable in the reconstructed image). The Whole Body phantom is composed of hot spheres (supported on cold cylindrical rods) whose centres are not co-planar, see Figure 3.2-4. It is used here to simulate oncology studies where the main interest is detecting hot spots.
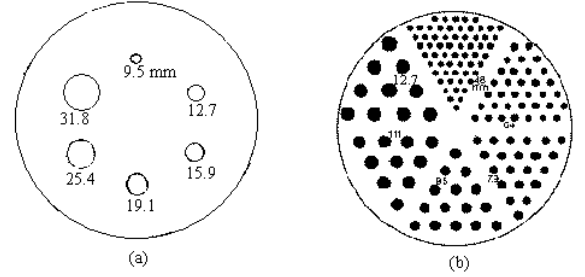

Figure 3.1-1: (a) Hot Spheres phantom. (b) Jaszczak phantom

The number of subsets was chosen equal to 14 for the GE Advance scanner and 24 for the PRT-1 scanner. The tuning parameter α in the stepsize formula for each of the OSMD and the OSCB algorithms is independent of the data and was chosen based on preliminary tests with a uniform cylinder phantom.

3.2 Phantom studies

3.2.1 Simulated data

For the Hot Spheres phantom, the hot ROI we considered is a union of the 3 largest circles in the central plane, the background ROI was taken as a circle of radius 52mm, located in the centre of the image. Figure 3.2-1 shows the reconstructed images after the second and tenth iterations. The trends in the coefficient of variation and contrast are presented in Figure 3.2-2. Note that all algorithms converge to the same CR, but OSEM increases CV dramatically over iterations.
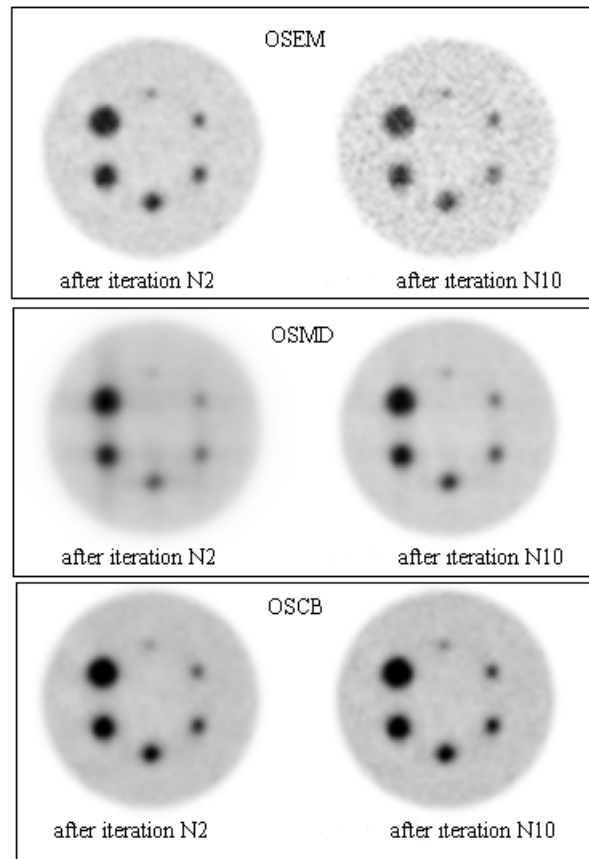
Figure 3.2-1: Comparison of the images reconstructed for the Hot Spheres phantom (PRT-1)
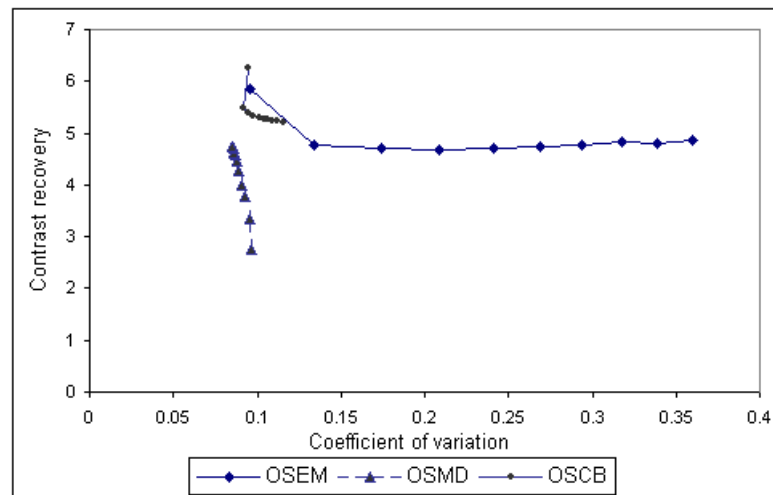

Figure 3.2-2: Trends in the coefficient of variation and contrast for the Hot Spheres phantom (PRT-1). Points represent results at different iteration number.

3.2.2 Acquired data

200 million and 50 million count acquisitions of the Jaszczak phantom were tested on the GE Advance scanner. The specific cold and hot ROI chosen for evaluation are circular regions in the central (18th) slice. The cold ROI is a union of 4 circles in the largest insert, each circle is of radius 6.3mm. The hot ROI (background) is located at the centre of the slice and has a radius of 36mm. Reconstructed images for all three algorithms look

quite the same and an example of such reconstructions is given in Figure 4.6-1. The trends in the coefficient of variation and contrast for the 50M count acquisition are presented in Figure 3.2-3.
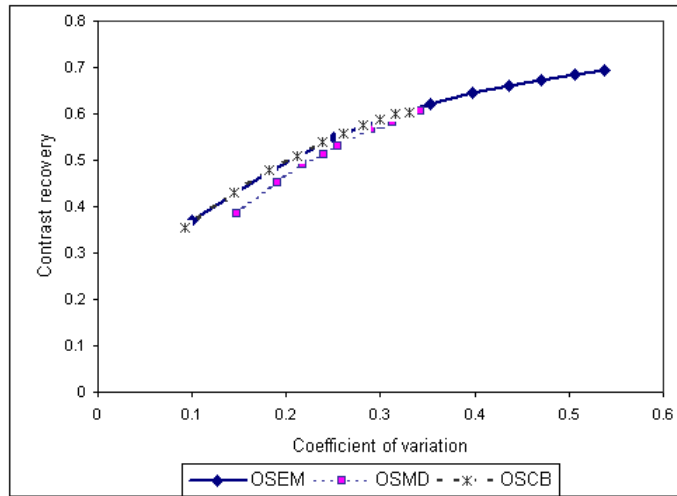

Figure 3.2-3: Trends in the coefficient of variation and contrast for the Jaszczak phantom (GE), with 50M counts

For the Whole Body phantom, a 10.78 million count acquisition was used. We considered a hot ROI of radius 24mm and a background ROI of 58mm. Figure 3.2-4 shows the Whole Body reconstructed images after the second and tenth iterations. The trends in the coefficient of variation and contrast vs. iteration number are presented in Figure 3.2-5.
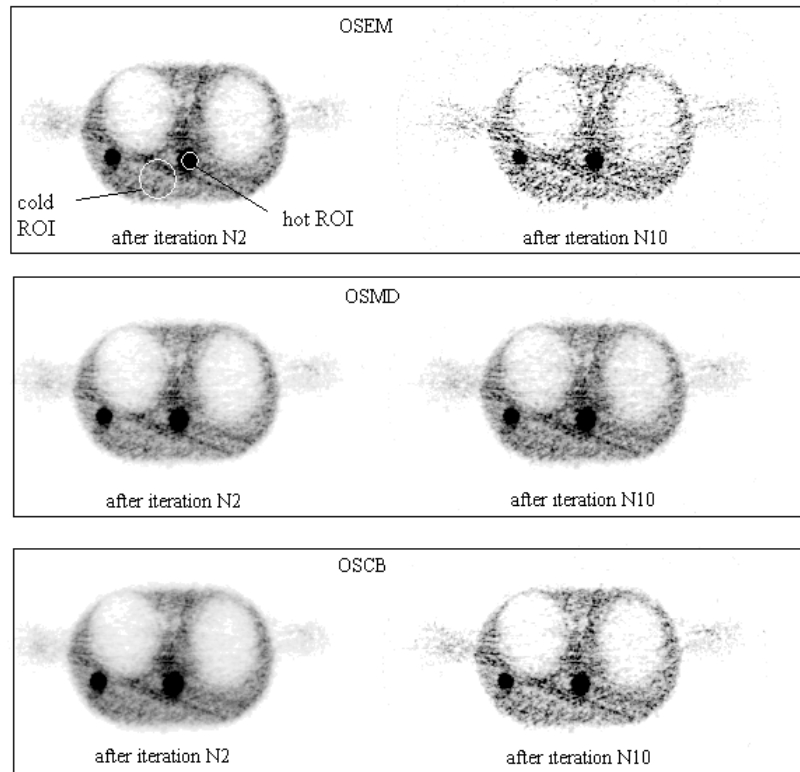

Figure 3.2-4: Comparison of the images reconstructed for the Whole Body phantom (GE)
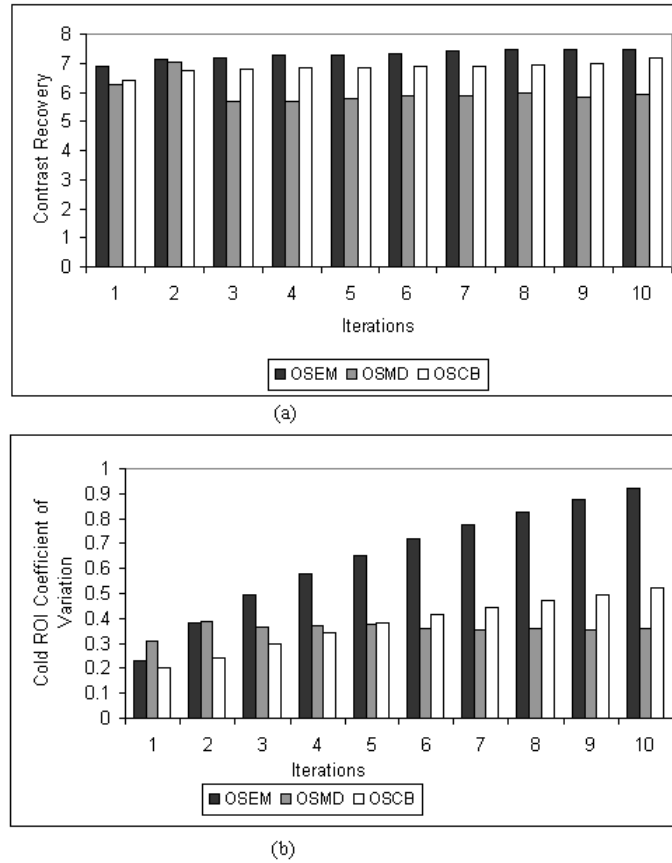
(a)

(b)

Figure 3.2-5 Trends in the coefficient of variation and contrast for the Whole Body phantom (GE)

3.2.3 Discussion

The results presented in the above figures show that:

- There is an evident trade-off between noise and contrast in all algorithms.

- In all the tests, images obtained by OSEM are much noisier than those obtained by OSMD and OSCB.

- For the OSEM algorithm the coefficient of variation grows strongly as more iterations are performed and in some cases, the image is essentially "destroyed" (see for example the tenth iteration in Figure 3.2-4). In OSMD and OSCB, on the other hand, the noise level is quite stable with respect to iteration number. In fact, a significant increase in the noise level can be seen only for the Jaszczak phantom, and even then it is moderate compared to OSEM

- In all algorithms, the contrast level is more or less the same, as can be expected since they all seem to converge to the "real" image. OSEM achieves the best contrast for the Jaszczak phantom. For the Whole Body phantom, OSEM and OSCB obtain the same contrast, while OSMD suffers from a lower contrast (note that in this test OSMD is less noisy than OSEM and OSCB and even succeeds in decreasing its noise level, unlike the others).

- In all algorithms, the contrast level remains stable during the iterations. Exceptions are the Jaszczak phantom, where OSEM increases its contrast at the expense of more noise, and the Hot Spheres phantom, where the contrast of OSMD grows, while the contrast of OSCB decreases (the last observation can be explained by the fact that

OSCB begins with a higher level of contrast, and at the tenth iteration it converges to the "true" contrast).

3.3 A clinical study

The algorithms were tested on clinical data of a woman with known stage T4 neoplasms of the breast and two metastases in the lung obtained by the PRT-1 scanner from the Hôpital Cantonal Genève. The reconstructions obtained by three algorithms are presented in Figure 3.3-1, showing that OSEM is significantly noisier than OSCB. The profiles of intensities shown in the figure correspond to a horizontal line drawn through the two points of interest (1 and 2). For all algorithms two peaks of higher intensity are separated from each other, but noise level is highest for OSEM.
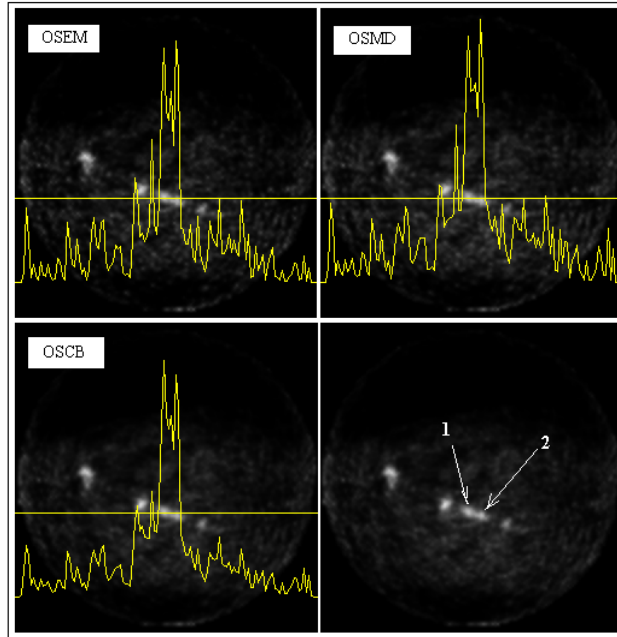

Figure 3.3-1: Comparison of the images reconstructed for an oncology study (PRT-1)

Table 3.3.1 shows the results of comparison between algorithms. The hot and cold ROI are of radius 6mm and 160mm respectively. The hot ROI is located around point 1 (see Figure 3.3-1) while the cold ROI is located lower down in the image.

As shown in Table 3.3.1 both regions have high non-uniformity. OSEM and OSCB reach the highest contrast, but OSEM gives the highest noise as in all other tests. The OSMD result is more uniform in the hot region but at the expense of less contrast. The OSCB algorithm gives the best trade-off between noise and contrast.

Table 3.3.1: Comparison of the reconstructions for the clinical study

Type of algorithm	Hot zone		Cold zone		Contrast
	Mean	CV	Mean	CV	
OSEM	1070	0.713	175	0.93	0.836
OSMD	1000	0.594	207	0.80	0.792
OSCB	1037	0.708	171	0.71	0.835

3.4 Conclusions

The new OSMD and OSCB algorithms adapted to the PET reconstruction problem, give generally high quality reconstructed images and compare well with OSEM - the most commonly used iterative algorithm. Both methods produce images which, compared to OSEM, are of higher uniformity with the expense of only a slight reduction in contrast. In addition, OSMD and OSCB remain stable with iteration number, unlike OSEM, which tends to deteriorate. This observation supports the better theoretical convergence properties of OSMD and OSCB and emphasises the fact that the actual number of iterations for OSEM should be selected carefully. In the single clinical study made here the OSCB algorithm is superior in both figures of merit, but of course, a more comprehensive study is needed for a clear conclusion.

4. Maximum-likelihood algorithms with filtering

In this section we discuss the evaluation of a modification of OSEM where filtering is introduced during the iterations. The reason for this modification is the well-known fact that (OS)EM images tend to deteriorate at large iteration number, especially for noisy data (see the previous section for results on OSEM).This deterioration shows that the Maximum Likelihood solution is not desirable with regard do visual quality and the FOMs under study. The filtering step is an attempt to regularise the solution (see section 5 for another way to introduce regularisation.) The main results in this section were presented in [Jac00].

Here, we experiment with an enhancement of OSEM for 3D PET reconstruction, which we call Inter-update Metz Filtered OSEM (IMF-OSEM). For details on the algorithm, see **D5.2** and [Jac00]. This enhancement incorporates not only smoothing action into the image updating process, but also feature amplification. Namely, the multiplicative image ordinarily used to update image estimates in OSEM is applied to a Metz-filtered version of the image estimate at certain intervals. A Metz filter has the property that it both attenuates high frequency noise and amplifies mid-range frequencies. When the amplifying mid-band is tuned to the frequencies of certain features in the underlying image, the filtering method drives the sequence of estimates toward an image in which these features are desirably accentuated.

We used the PARAPET software to test the performance of IMF-OSEM relative to un-filtered and post-filtered OSEM on phantom data acquired on the GE Advance scanner [GEMS]. In some settings (e.g. [Sli98], for SPECT), it has been found that filtering between iterations in EM yields similar results as post-filtering. Since IMF-OSEM applies filters in a similar way, it is natural to compare its performance with post-filtering as well. Comparison was also made with the commercial 3DRP software for the scanner (an implementation of PROMIS [Kin89]). Performance was measured in terms of the trade-off between contrast and noise. For low count acquisitions, IMF-OSEM was found to perform better than the other algorithms when the parameters of the Metz filter were suitably tuned to the size of the object to be enhanced. The level of improvement of IMF-OSEM over post-filtering seemed to increase as the acquisition statistics decreased.

4.1 Data and procedures

A qualitative study was performed on a simulation of a very noisy acquisition of the Utah phantom on the PRT-1 scanner. PARAPET Promis software was used with varying values of the α parameter of the Hanning window to get more or less smoothing. Results were compared with IMF-OSEM with different settings for the power of the Metz filter. The objective of this study was to see what settings for the parameters are sensible for this particular noise level.

Quantitative studies were made of a Jaszczak phantom and an axially asymmetric Whole Body phantom. All projection data were pre-corrected for attenuation, detector efficiency, scatter, and randoms.

In our analysis, we examined the trade-off between CR and the background CV for hot and cold phantom lesions of different sizes. Three Metz filter parameter choices for IMF-OSEM were tested and were compared to OSEM post-filtered by the same filter. Axial and transaxial Metz filters were chosen to have a common Metz power N=1. This value was empirically found to lead to good visual quality and a reasonable regime for testing the effect of different FWHMs for a wide range of acquisitions. The filter FWHMs are expressed in centimetres and are denoted XF (x-direction FWHM) and ZF (z-direction FWHM) respectively. Based on some preliminary tests, the number of subsets was set to 14 and all inter-update filters in IMF-OSEM were applied at intervals of full iterations.

The 3DRP reconstructions were made on a 256 by 256 transaxial image grid with a field of view radius of 55 cm. Three filter configurations were tested. Filter configurations in the GE 3DRP software are specified by a 'Hanning' parameter for transaxial filtering and a 'Ramp' parameter for axial filtering and are given in centimetres throughout this section.

4.2 Jaszczak Phantom Study

200 million count and 50 million count acquisitions of the Jaszczak phantom were made and for each acquisition, trends in CR vs. CV were measured for cold lesions of diameter 1.27 cm and 0.64 cm. The lesions corresponded to transaxial cross-sections of the phantom's cold-inserts. ROIs for measuring local and background means were each composed of 3 circular sub-ROIs of radius 0.4 cm. Three sub-ROIs were centred in cold inserts while three others were placed in the background of the same sector.

The measured CR vs. CV trends are plotted in Figure 4.2-1 till Figure 4.2-4. In general, we observe that for a given noise level, IMF-OSEM achieves superior contrast as compared to plain and post-filtered OSEM. The level of improvement appears to increase as the number of counts in the acquisition is lowered and as the filter FWHMs are adjusted to the size of the lesion. In particular, for the 0.64 cm lesion, for which the FWHMs are comparatively large, one sees a narrower margin of improvement than for the 1.27 cm lesion.

As observed in Figure 4.2-2, when the FWHMs are comparable to the dimensions of the insert containing the lesion, enlarging the FWHMs can reduce noise level. However, enlarging them excessively smears the lesion, such that noise is reduced at a significant expense in contrast and, in some cases, at the expense of the contrast-noise ratio attained. This is apparent from Figure 4.2-3 and Figure 4.2-4 for XF=0.8 cm.

For low count acquisitions, we see also that IMF-OSEM outperformed 3DRP for several of the Metz filter parameter choices tried.
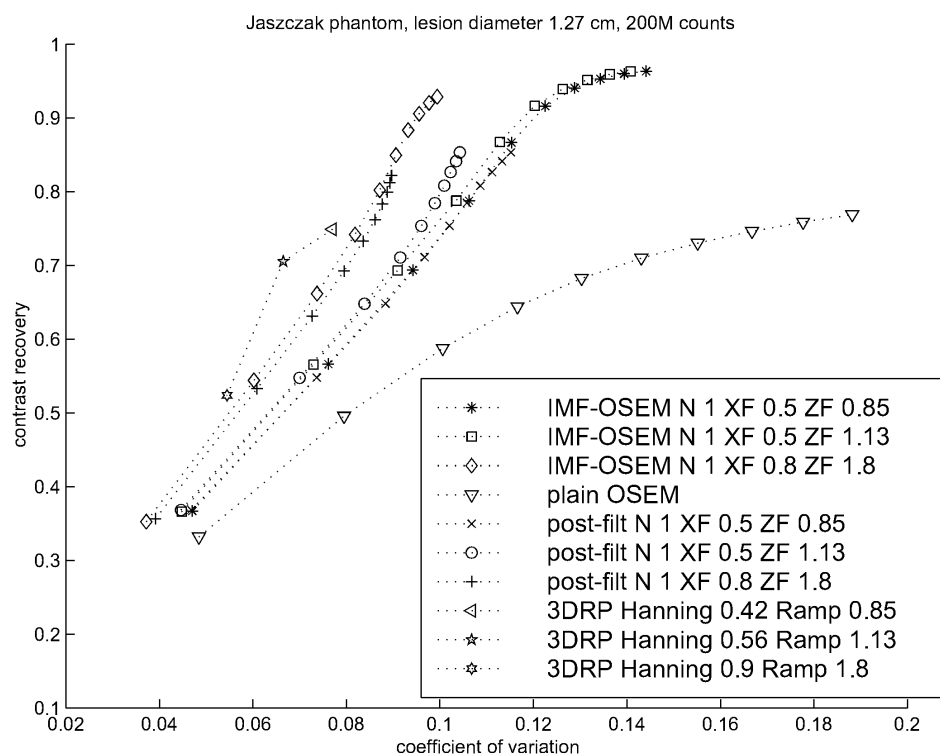
Figure 4.2-1: Trends in contrast recovery vs. background noise for a high count Jaszczak phantom acquisition, measured for the 1.27 cm cold inserts.
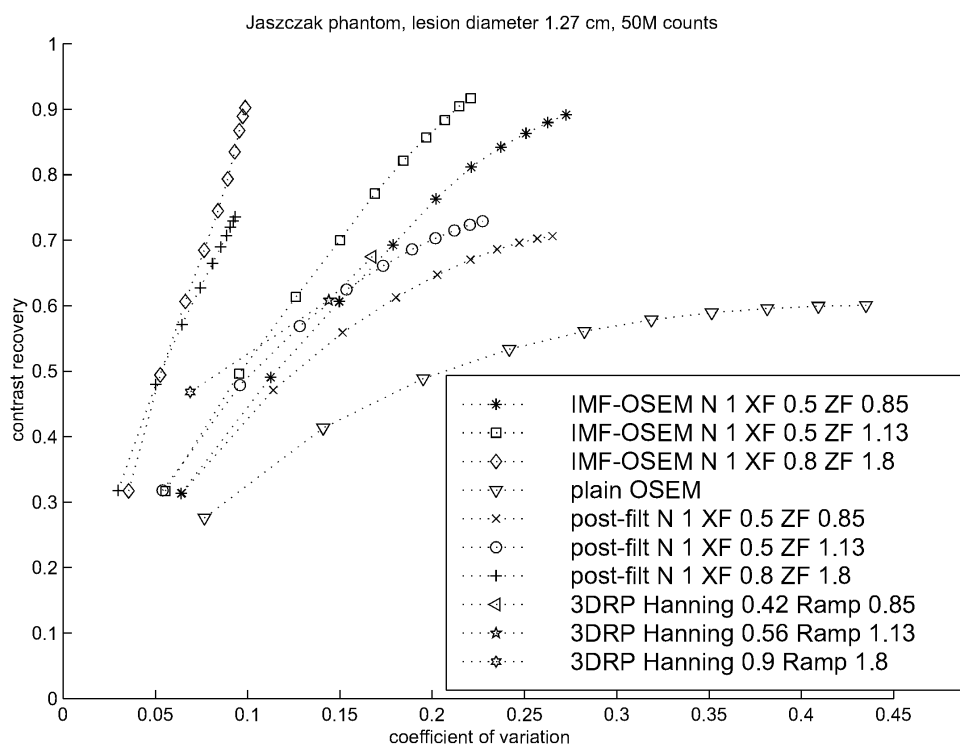

Figure 4.2-2: Trends in contrast recovery vs. background noise for a low count Jaszczak phantom acquisition, measured for the 1.27 cm diameter cold inserts.

Jaszczak phantom, lesion diameter 0.64 cm, 200M counts

IMF-OSEM N 1 XF 0.5 ZF 0.85
IMF-OSEM N 1 XF 0.5 ZF 1.13
IMF-OSEM N 1 XF 0.8 ZF 1.8
plain OSEM
post-filt N 1 XF 0.5 ZF 0.85
post-filt N 1 XF 0.5 ZF 1.13
post-filt N 1 XF 0.8 ZF 1.8
3DRP Hanning 0.42 Ramp 0.85
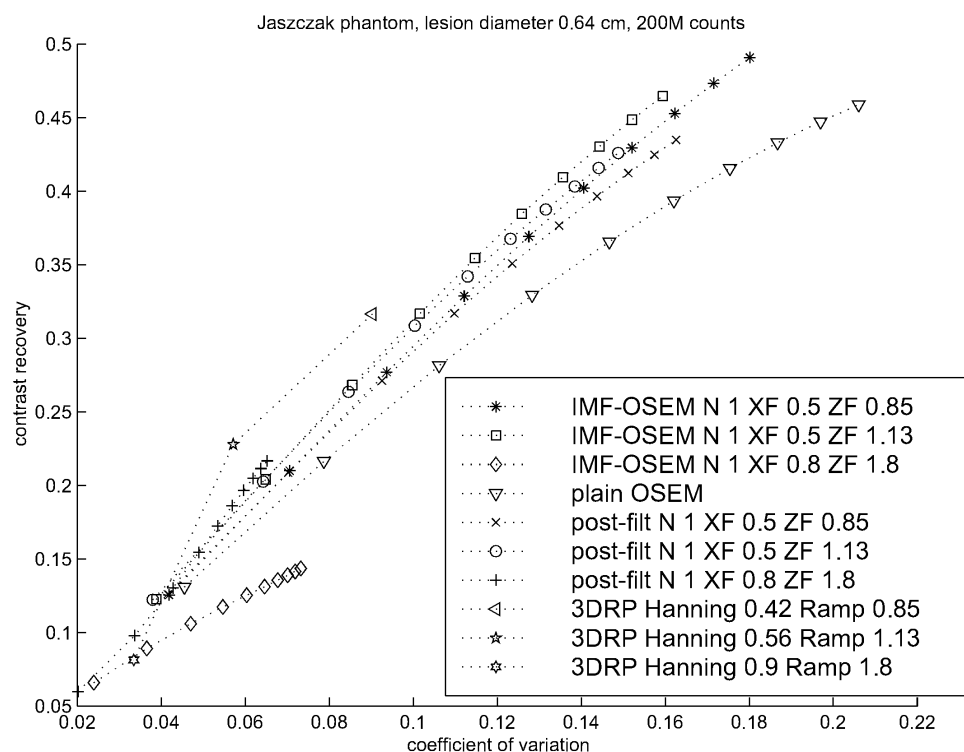3DRP Hanning 0.56 Ramp 1.13
3DRP Hanning 0.9 Ramp 1.8

Figure 4.2-3: Trends in contrast recovery vs. background noise for a high count Jaszczak phantom acquisition, measured for the 0.64 cm diameter cold inserts.
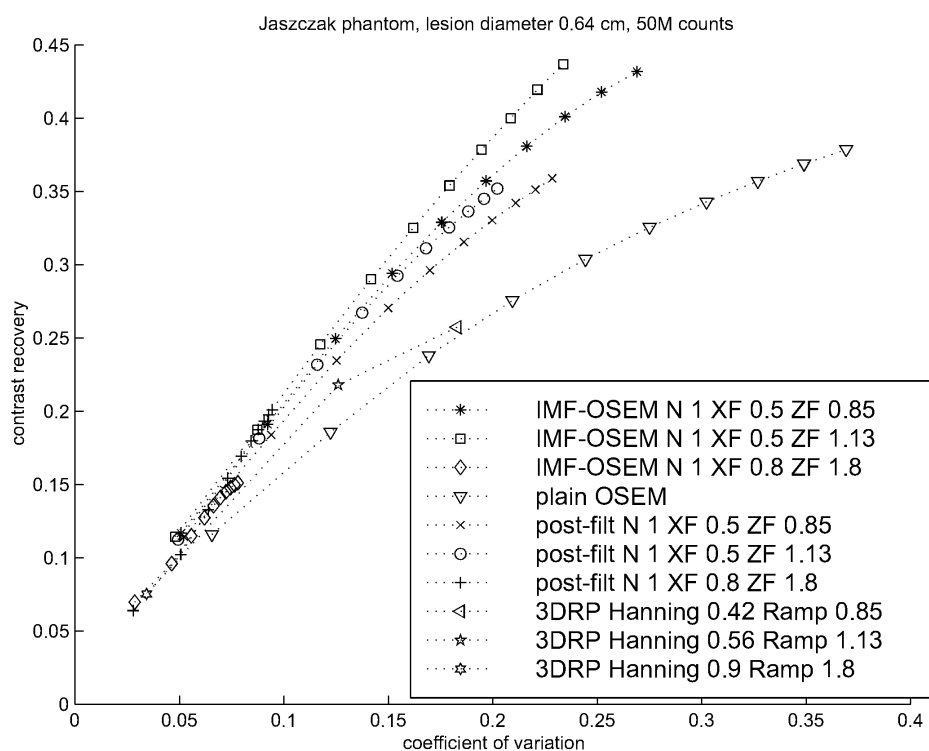
Jaszczak phantom, lesion diameter 0.64 cm, 50M counts

IMF-OSEM N 1 XF 0.5 ZF 0.85
IMF-OSEM N 1 XF 0.5 ZF 1.13
IMF-OSEM N 1 XF 0.8 ZF 1.8
plain OSEM
post-filt N 1 XF 0.5 ZF 0.85
post-filt N 1 XF 0.5 ZF 1.13
post-filt N 1 XF 0.8 ZF 1.8
3DRP Hanning 0.42 Ramp 0.85
3DRP Hanning 0.56 Ramp 1.13
3DRP Hanning 0.9 Ramp 1.8

Figure 4.2-4: Trends in contrast recovery vs. background noise for a low count Jaszczak phantom acquisition, measured for the 0.64 cm diameter cold inserts.

4.3 Whole Body Phantom Study

The Whole Body phantom is composed of hot spheres (supported on cold cylindrical rods) whose centres are not co-planar, see Figure 4.3-5. A 10.78 million count acquisition was made with the hot spheres filled with F-18 tracer and with faster-decaying C-11 tracer in the background. A second higher contrast acquisition was made 20 minutes later with approximately the same number of counts.

For the low contrast acquisition, we carried out the same CR vs. CV as in the previous subsection on 3 hot lesions and a cold lesion. In this case, hot lesions corresponded to cross-sections of the spheres and the cold lesion corresponded to a cold support cross section. For hot lesions, circular ROIs approximately equal in diameter to the internal diameter of the spheres were used to cover the lesion. The cold lesion ROI diameter was approximately equal to the diameter of the support. Background ROIs of approximately 4 cm in diameter were placed in the same plane as the corresponding lesion.

The trends in the plots show many of the same patterns as in the Jaszczak phantom study. For a given noise level, IMF-OSEM outperformed plain and post-filtered OSEM in terms of contrast recovery. In most cases also, a choice of Metz filter parameters was found which lead to better performance than 3DRP.

As before, the level of improvement of IMF-OSEM over the other iterative algorithms is correlated with how well matched the FWHMs are to the geometry of the feature containing the lesion. This is observed in Figure 4.3-1-Figure 4.3-3 for the case XF=0.5 cm for which the best relative improvement is observed for the 1.25 cm hot lesion, but is less both for the smaller 0.8 cm lesion and the larger 3.4 cm lesion.

When the FWHMs are large, oversmoothing results in reduced noise at a significant expense in contrast (as for ZF=1.8 cm). Conversely, as seen for the 3.4 cm hot lesion, reconstructions with relatively small FWHMs do not yield significant enhancement. Indeed all filtered algorithms using FWHMs less than one third the diameter of the feature reached similar noise and contrast levels in this case. This is expected since features which are large compared to the FWHMs of the filter consist of frequencies lying in the low-frequency band of the filter, where neither amplification nor attenuation occurs. Hence the filtering action does not influence them.
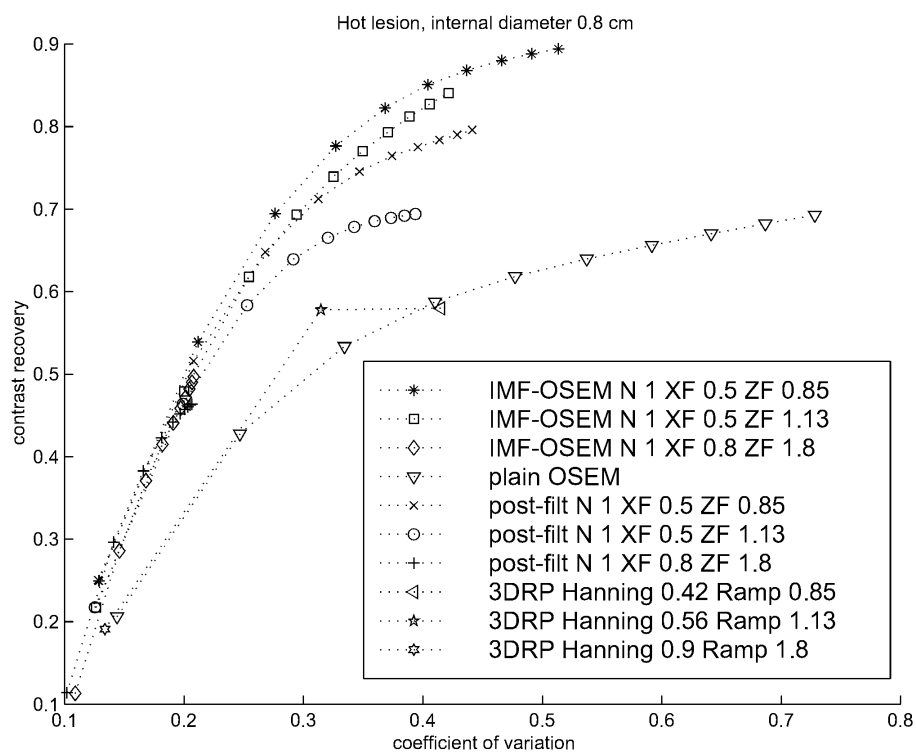
Hot lesion, internal diameter 0.8 cm

Figure 4.3-1: Trends in contrast recovery vs. background noise for a low count, low contrast Whole Body phantom acquisition, measured for a 0.8 cm hot lesion.
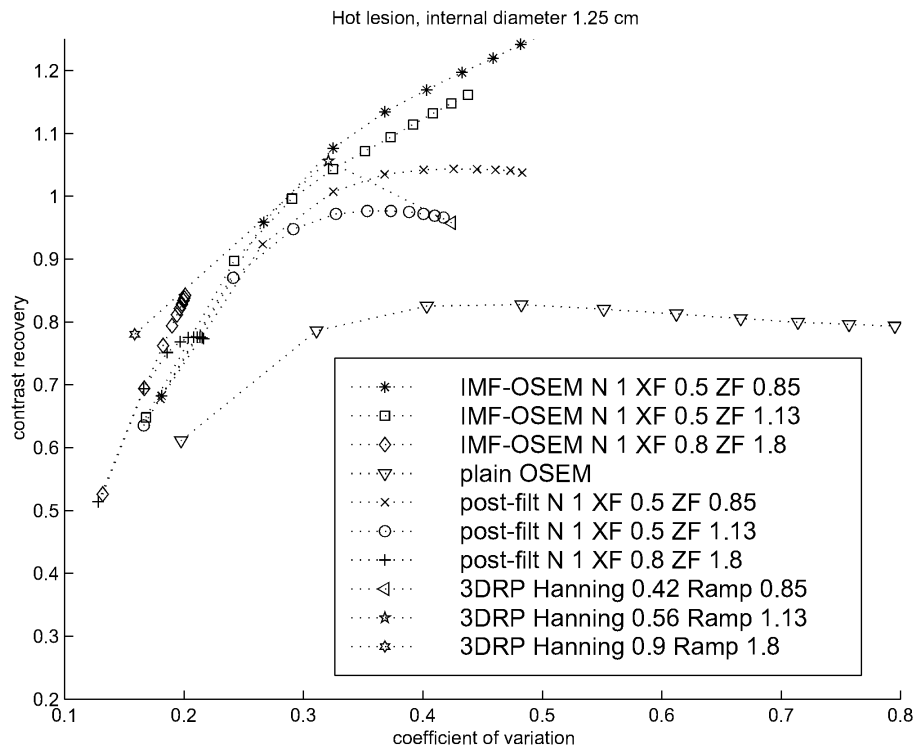
Hot lesion, internal diameter 1.25 cm

Figure 4.3-2: Trends in contrast recovery vs. background noise for a low count, low contrast Whole Body phantom acquisition, measured for a 1.25 cm hot lesion.
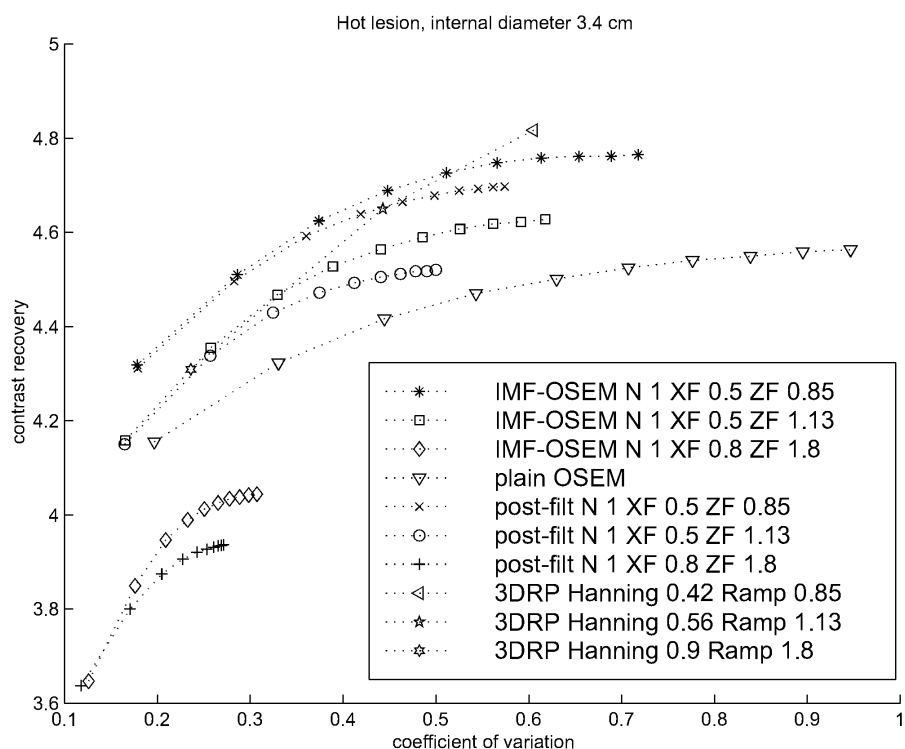
Hot lesion, internal diameter 3.4 cm

Figure 4.3-3: Trends in contrast recovery vs. background noise for a low count, low contrast Whole Body phantom acquisition, measured for a 3.4 cm hot lesion.
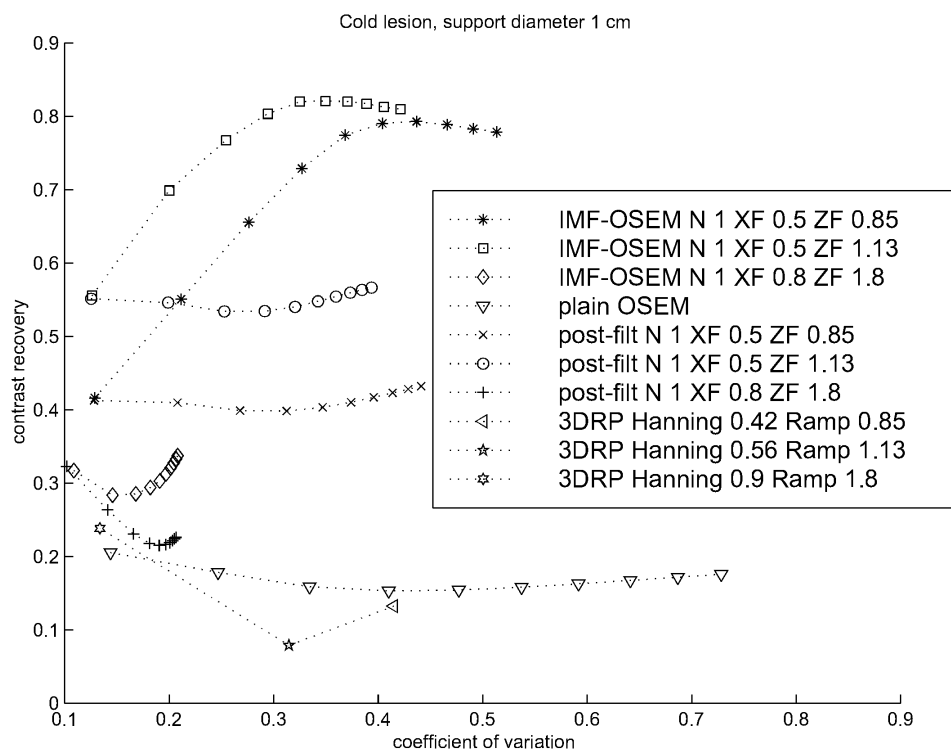
Cold lesion, support diameter 1 cm

Figure 4.3-4: Trends in contrast recovery vs. background noise for a low count, low contrast Whole Body phantom acquisition, measured for a 1 cm cold lesion.

For the higher contrast acquisition, we found interesting qualitative results (Figure 4.3-5) when comparing OSEM, IMF-OSEM with N=0, and IMF-OSEM with N=1. The value N=0 corresponds to Gaussian filtering, which is more conventional for smoothing than Metz filters. We see that certain cold lesions (marked by the white arrow) are visible only via Metz filtering.
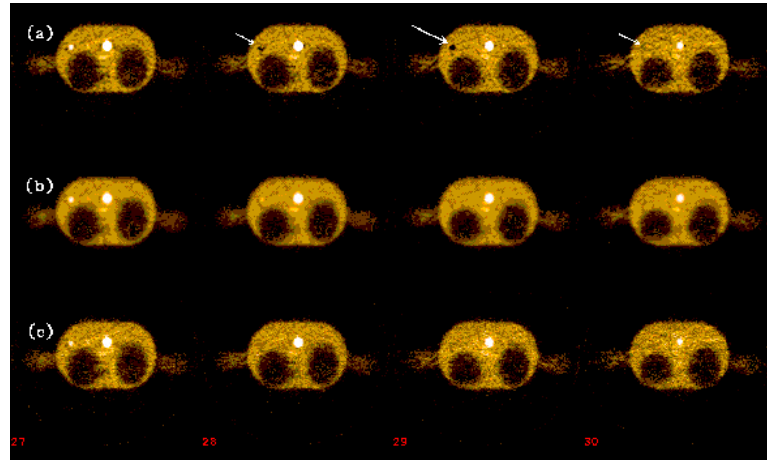

Figure 4.3-5: Four slices of Whole Body phantom reconstructions after 2 full iterations and using 14 subsets (a) IMF-OSEM with non-trivial Metz filter: N=1 XF=0.5 ZF=0.85 (b) IMF-OSEM with Gaussian filter: N=0 XF=0.5 ZF=0.85 (c) plain OSEM.

4.4 Utah Phantom study

The simulation (generated using the Eidolon software) consisted of 600k counts (no randoms, but including scatter)[3]. Activity ratios in the compartments were 0:1:2 (see Figure 4.4-1). Sample image reconstructions are presented in Figure 4.4-1 and Figure 4.4-2.

Promis reconstructions used cut-off at Nyquist, and α equal in both axial and transaxial direction. Visually it is obvious that for such low count studies, a smoothing window has to be used to get a good Promis reconstruction.
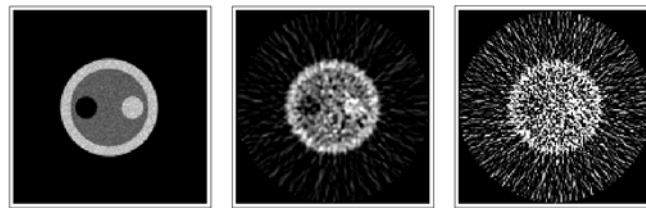

Figure 4.4-1: One plane near the middle of the scanner of the Utah phantom. Left: detected counts generated by the simulator; Middle: Promis with Hamming window (α=0.5); Right: Promis with rectangular window (α=1). Negative values are truncated to 0.

We compared unfiltered EM with unfiltered OSEM with 6 subsets. Images (and FOMs) were virtually indistinguishable when 1 EM iteration was compared with 1 OSEM subiteration. This confirms the well-known observation that for the first iterations, OSEM gives a time-saving of about the number of subsets, at least for a small number of subsets. Then we compared different Metz powers (denoted by *N*) for a fixed FWHM of 1cm. This value was arbitrarily chosen. Note that the FWHM is not at all optimised towards the

---

[3] We analysed both attenuation-precorrected data and uncorrected data where we took the attenuation into account in the sensitivity matrix (see **D5.2**). However, for this particular set-up there was no appreciable difference between the two procedures, probably because the phantom is only 20cm diameter, and placed exactly in the centre of the scanner.

size of the features in the image, as the inner cylinders have a diameter of 4.5cm. In this section, both filter FWHM and power were kept the same in axial and transaxial direction.

Visually, it is obvious that some kind of filtering has to be done for very low count studies . Also, a Metz power $N=1$ gives unacceptable artefacts in this case. On the other hand, with a power $N=0$ (i.e. a Gaussian filter) the image is very smooth.
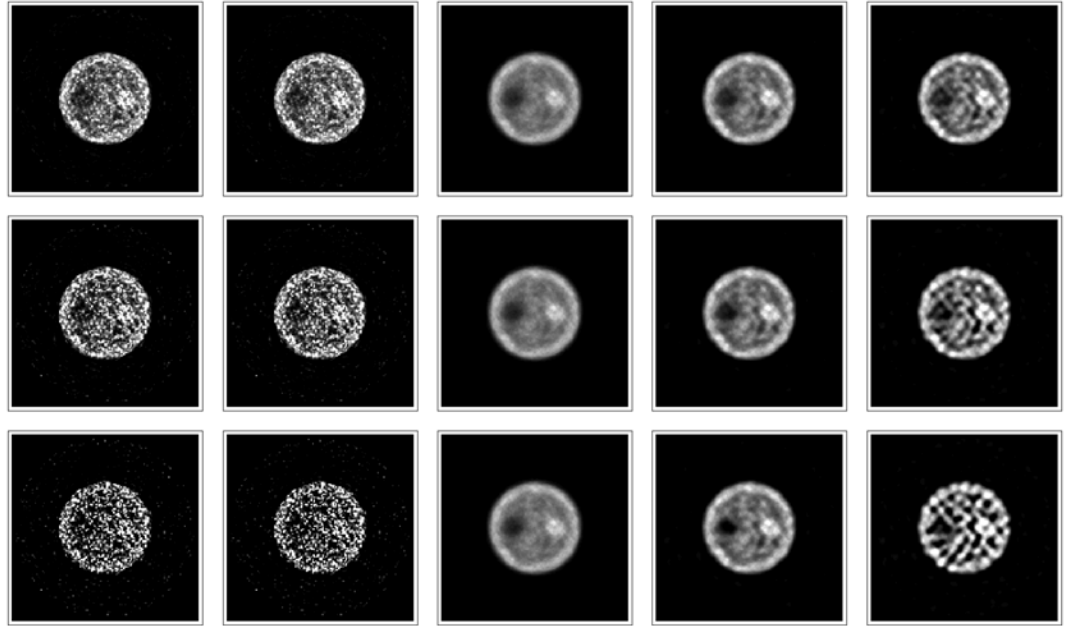

Figure 4.4-2: Iterative Reconstructions of the Utah phantom, same plane as previous figure. Top row: 24 subiterations; middle row: 48 subiterations; bottom row: 128 subiterations. Columns: (1) unfiltered EM, (2) unfiltered OSEM, (3) IMF-OSEM N=0, (4) IMF-OSEM N=0.5, (5) IMF-OSEM N=1. (See text)

We confirmed this also by taking horizontal profiles. Promis data show large negative values due to inconsistencies in the noisy data. IMF-OSEM with $N=0$ fails to resolve the cold feature in the image because it oversmooths the image. Power $N=1$ has very good contrast but overshoots any edges considerably.
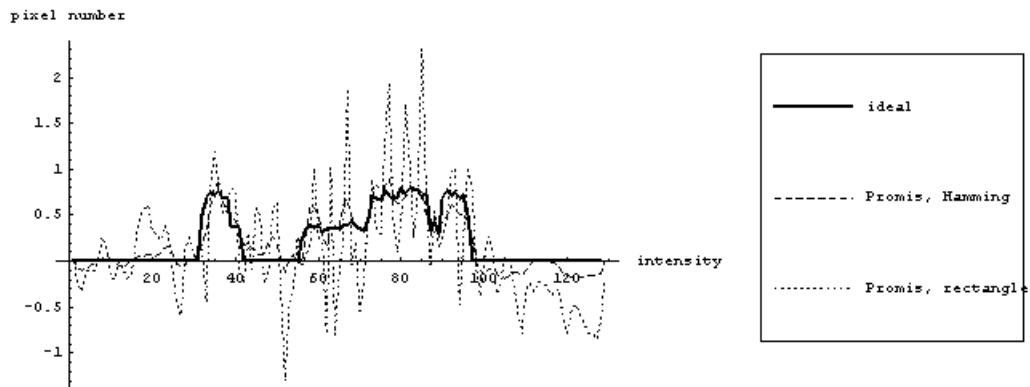

Figure 4.4-3: Horizontal profile through the same slice. Comparing the ideal image with Promis reconstructions with $\alpha=1$ and $\alpha=0$.
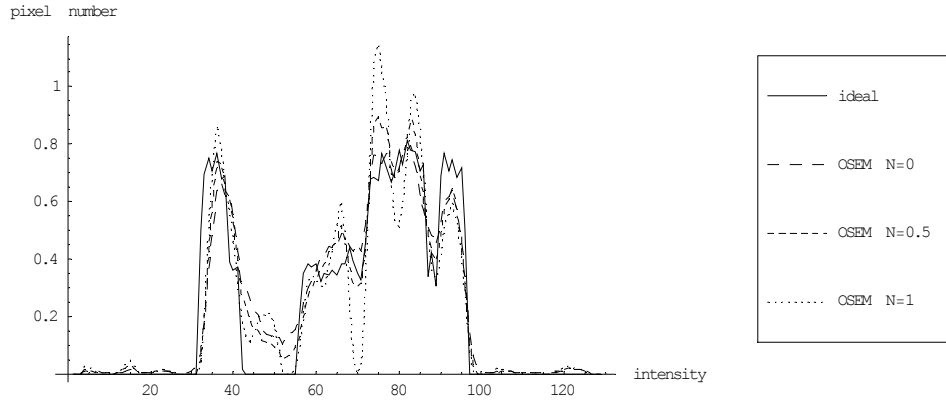
Figure 4.4-4: Same profile as previous picture, but now through IMF-OSEM reconstructions with varying Metz power (48 subiterations).

This qualitative analysis shows that for (very) noisy data that filter parameters have to be chosen carefully in terms of the quality of the acquired data. This is true for both analytic and iterative algorithms.

The amplifying capability of the Metz filter raises a potential hazard in noisy data reconstructions. If the FWHM parameters of the filter are set too low, the amplifying mid-band of the filter may be shifted to too high a range where it acts upon noise instead of or in addition to the features of the underlying image. In this case, IMF-OSEM may iteratively amplify noise with catastrophic results for the reconstruction. We confirmed this by taking larger FWHM (data not shown), making the artefacts disappear. However, such a large FWHM would be problematic when smaller features are present.

The amplify-and-smooth approach exploited by Metz is based on an assumption of tuning flexibility. Namely, we suppose that the filter can be tuned so that its amplifying midband coincides with the features of the underlying image while the attenuating high band coincides with the noise frequencies. In very noisy acquisitions, the frequency range of the noise and the underlying image approach one another making this division difficult. It is entirely likely that for sufficiently low statistics, the Metz filter does not have enough degrees of freedom to permit this kind of tuning. In this case, one must search for more flexible amplify-and-smooth filters. Furthermore, adaptive methods for determining the division point between image and noise frequencies become increasingly important.

4.5 Conclusions on IMF-OSEM

With acquired phantom data, we have tested the performance of IMF-OSEM against plain and post-filtered OSEM in a common implementational framework. In addition, IMF-OSEM's performance was compared with that of commercial 3DRP software. Trends in contrast recovery vs. coefficient of variation for low count acquisitions showed that IMF-OSEM, with judiciously chosen parameters, achieves substantially better contrast for a given noise level than all the other algorithms. Visual evidence of this enhancement capability also manifested in a Whole body phantom study where plain OSEM failed to reveal a feature while IMF-OSEM revealed it quite clearly.

We have found that the level of enhancement of IMF-OSEM is most significant when the filter parameters are adjusted to the geometry of a particular feature to be enhanced. Quantifying the optimum choice of parameters will be the subject of future investigation. Additionally, we would like to see if the inter-update filtering technique discussed here may be extended to enhance features of multiple sizes and geometries. We speculate at this time that this may be done using linear combinations of different Metz filters, where the parameters of each Metz filter are tuned to the size of a different feature.

4.6 Application to OSMD and OSCD

The OSMD and OSCB algorithms can use the same Metz filter, which may be applied to a corrected (new) image after each full iteration of the algorithm. This option was used in our study[4]. Examples of reconstruction of the Jaszczak phantom, with and without iterative filtering, are presented in Figure 4.6-1.
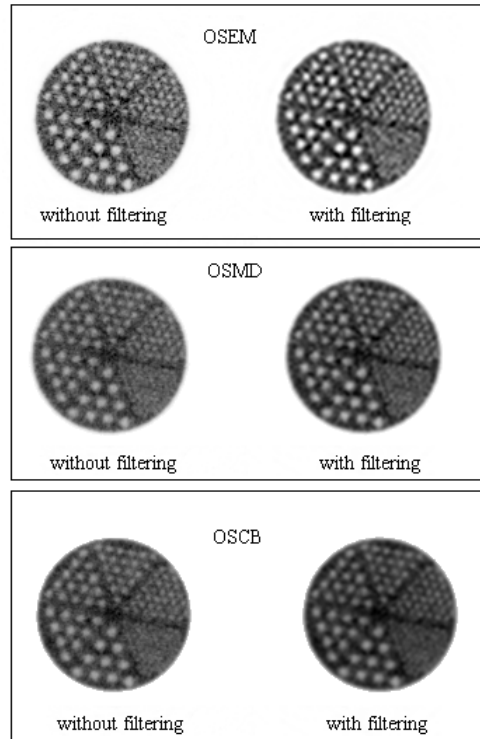

Figure 4.6-1 Comparison of the image (5 full iterations) for the Jaszczak Phantom (GE, 200M counts) by OSEM, OSMD and OSCB with and without filtering

The superiority of iterative Metz filtering for all reconstructions is evident. It significantly improves the contrast and decreases the noise in all regions except for the region with the smallest inserts. The use of Metz filtering diminishes the differences between the algorithms, but the main relation is still valid: the highest noise level is reached by OSEM, which on the other hand has slightly better contrast.

5. Bayesian algorithms

Another way to regularise the ML-solution is by using prior information. This section discusses the evaluation of the Median Root Prior, implemented as discussed in **D5.4.** The material from this section is taken from [Bet00].

Recently S. Alenius and U.Ruotsalainen have proposed the Median Root Prior [Ale97] as a penalty function for the MLEM. The general assumption of the method is that the desired image is locally monotonic. By setting the penalty of a pixel against the local median, the penalty is set only if inside a local neighbourhood the image contains non-monotonic structures. This corresponds to the main properties of median filtering where images that are invariant under the filtering are called root images, and they are locally monotonic. The algorithm has been successfully evaluated with 2D PET data showing very interesting properties both in terms of noise reduction, quantitative accuracy, and convergence [Ale98].

---

[4] Both OSMD and OSCB do not lend themselves to the same form of inter-update filtering as OSEM.

We evaluated the 3D OSEM-MRP algorithm using experimental phantom data simulating PET brain studies in terms of shape and size. High (200Mcounts) and low (< 50Mcounts) count statistics 3D PET were acquired. The performance of the algorithm was evaluated by calculating simple figures of merit (contrast, coefficient of variation, activity ratio between two regions). The results obtained with 3D OSEM-MRP were compared with those obtained using a "pure" 3D OSEM and the PROMIS algorithm using different transaxial and axial reconstruction filters.

5.1 Phantom Studies

Four different phantoms were considered for the evaluation of the algorithm: a uniform cylindrical phantom (UCY), the Jaszczak phantom (JZA), the 3D Hoffman brain phantom (HB) (Data Spectrum Corporation) and the striatal phantom (ST) (RSD Radiology Support Devices, Long Beach, CA). Each of these phantoms brain like structures and thus allow evaluation of the performance of the algorithm for 3D PET brain studies.

5.1.1 UCY phantom

A UCY phantom (diameter = 20cm, height = 20cm) was filled with a homogeneous solution of water and 18F. The phantom was positioned in the centre of the scanner Field Of View and two acquisitions: EM1(200Mcounts) and EM2 (10Mcounts) were performed.
A "pre-injection" high statistics transmission scan of 30 min was used for attenuation correction.

5.1.2 JZA phantom

The JZA phantom with cold rods sectors was filled with a homogeneous solution of water and 18F. The diameters of the cold rods are 12.7, 11.1, 9.5, 8.4, 6.4, 4.5 mm. The phantom was positioned in the centre of the scanner FOV and two acquisitions: EM1(200Mcounts) and EM2 (50Mcounts) were acquired.
A "pre-injection" high statistics transmission scan of 30 min was used for attenuation correction.

5.1.3 HB phantom

The HB phantom was filled with a homogeneous solution of water and 18F. The phantom was positioned in the centre of the scanner FOV and one acquisition: EM1 (200Mcounts) was performed with comparable statistics for a standard 3D PET 18F[FDG] brain study.
A "pre-injection" high statistics transmission scan of 30 min was used for attenuation correction.

5.1.4 ST phantom

The ST phantom was filled (both for background (bckg) and "subcortical structures" (SS) with a homogeneous solution of water and 18F. Ratio of activity between SS and background was 3.84 (activity concentration at the start of the scan was 43.4 kBq/ml for the SS and 11.3 kBq/ml for the background). The phantom was positioned in the centre of the scanner FOV and one acquisition: EM1 of 33Mcounts was performed with comparable statistics acquired in 3D PET 18F[FESP] studies.
A "pre-injection" transmission scan of 10 min was used for attenuation correction.

5.2 Phantom data analysis - Figure of Merit (FOM)

Data evaluation was performed calculating a simple FOM for each phantom.

5.2.1 UCY

A single ROI with a diameter of 15.0cm was drawn in each slice of each reconstructed image set. Mean, Standard Deviation (SD) and Coefficient of Variation (CV) =(SD/Mean) were calculated for each ROI.

5.2.2 JZA phantom

For each cold rod sector of the JZA phantom ROIs of the same diameter of the cold lesions were drawn in each lesion of each sector with the exception of the smallest one (4.8mm). 20 ROIs with diameter of 6mm were drawn in the hot background of the phantom. Contrast (CR_{cold}) and CV (only for the background activity) were calculated for each sector of the phantom.

5.2.3 HB phantom

The digital version of the 3D HB phantom was registered and resliced to the reconstructed experimental images. Registration and reslicing was performed using a surface matching technique as implemented in the *Analyze* software. ROIs were drawn on two representative slices of the digital phantom and then transferred onto the reconstructed experimental data.
Circular ROIs with diameter of 5-6mm were drawn over the "grey" (20 -30 ROIs) matter and "white" (15 -20 ROIs) matter.
Activity Ratio (AR) between grey and white mean values was calculated for the two slices as well as the CV for the grey and white matter.

5.2.4 ST phantom

ROI analysis was performed in the same way as for the HB phantom.
6 ROIs with a diameter of 4.5mm were drawn over the "putamen", 2 ROIs over the "caudate", and 20 ROIs in the hot background.
AR between "putamen" and background as well as for the "caudate" and background were calculated while CV was calculated only for the background activity.

5.3 Algorithms and Reconstruction set-up

All the studies were reconstructed using the following set-up of parameters:

Image Matrix 281 x 281 x 35 (pixel size 1.95mm, corresponding to the arc-corrected bin size of the scanner).

OSEM and OSEM-MRP

14 subsets, β = 0.3, 0.5 and 0.9, two-dimensional (2DM) and full three-dimensional (3DM) median filters of width 3 were used. In the following graphs, Wx, Wy, Wz refer to the width of the median in each direction, so Wz=1 refers to 2DM.

PROMIS

The following reconstruction parameters were used (cut-off for all filters was at Nyquist).

	Transaxial Filter	Axial Filter
Promis$_{RR}$	Rectangular	Rectangular
Promis$_{HR}$	Hanning	Rectangular
Promis$_{HH}$	Hanning	Hanning

These three conditions were chosen to cover a wide range of possible reconstruction set-ups used for clinical studies. Condition 1 allows the best resolution to be maintained in the images but usually with too high noise. Condition 2 is a good compromise in term of some noise reduction in the transaxial plane still maintaining "good" resolution in the axial direction. Condition 3 represents a typical set up used in clinical application particularly in case of very low statistic data.

5.4 Results

5.4.1 UCY phantom

Figure 5.4-1 and Figure 5.4-2 report the CV as a function of the iteration number for high (EM1) and low statistics (EM2). While OSEM clearly does not converge (within the 140 iterations considered) and shows a typical increase of the noise as the iterations proceed, OSEM-MRP shows a clear tendency to converge to a stable solution for both high and low statistics. With respect to Promis reconstruction OSEM-MRP can achieve higher or lower CV depending on the parameter configuration used in the reconstruction. When comparing the 3DM with the 2DM median filter, we see that the first seems to result in faster convergence.
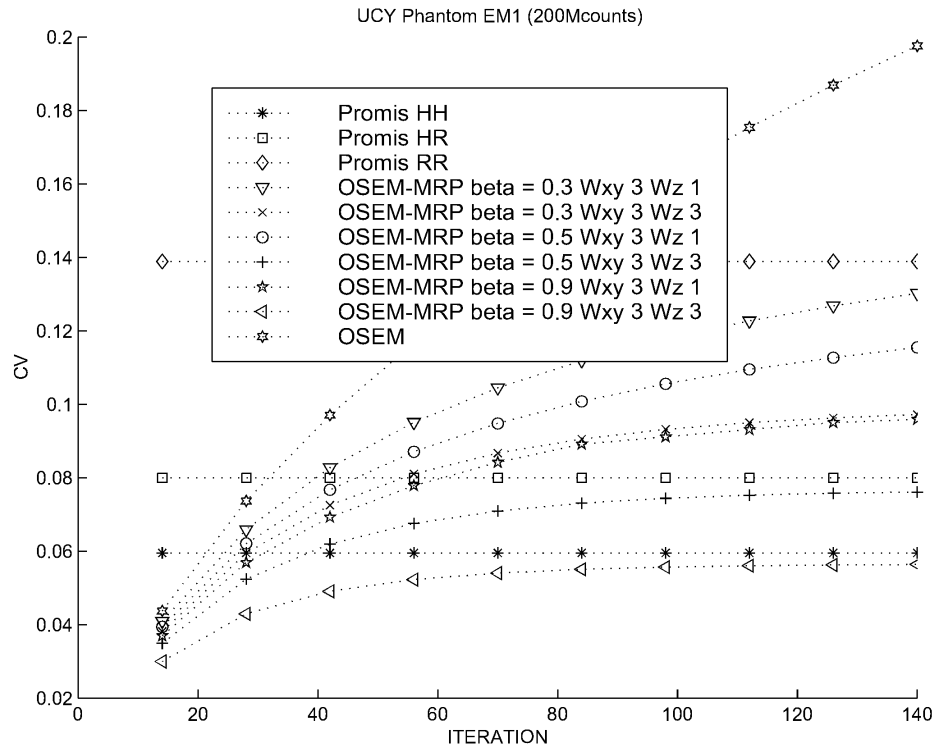
Figure 5.4-1: UCY phantom with high statistics. CV as a function of iteration number for all algorithms and reconstruction set-ups. Promis results are reported over iterations only for an easy comparison with OSEM and OSEM-MRP
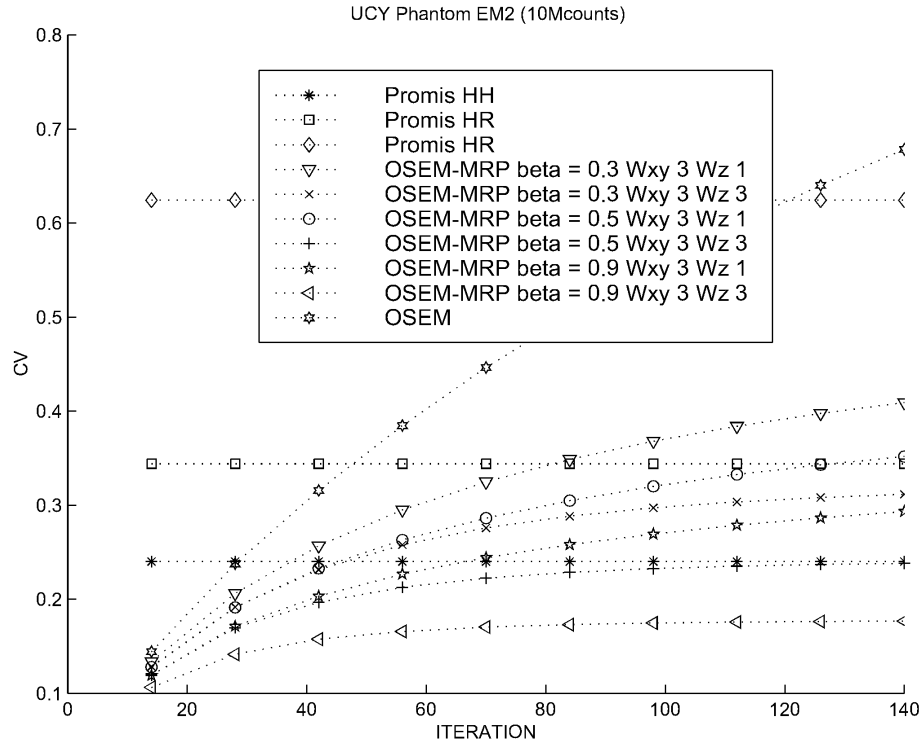
Figure 5.4-2: UCY phantom with low statistics. CV as a function of iteration number for all algorithms and reconstruction set-ups. Promis results are reported over iterations only for an easy comparison with OSEM and OSEM-MRP.

5.4.2 JZA phantom.

Figure 5.4-3 and Figure 5.4-4 report contrast as a function of CV for the low statistics (EM2) data calculated for sectors with cold lesions of 12.7 and 6.4mm. The results show that PromisRR and OSEM gives higher contrast but as expected also with higher noise. Furthermore OSEM has not reached convergence after the 140 iterations here considered. Compared with PromisHR and PromisHH, OSEM-MRP provide good results both in terms of contrast and CV. PromisHH maintains the same contrast as PromisHR, due to the particular axial symmetry of the phantom along the Z direction, but with a noticeable reduction of the noise. OSEM-MRP2DM has higher contrast with respect to PromisHH and PromisHR but with a higher CV while OSEM-MRP3DM has an intermediate behaviour depending on the β value used.
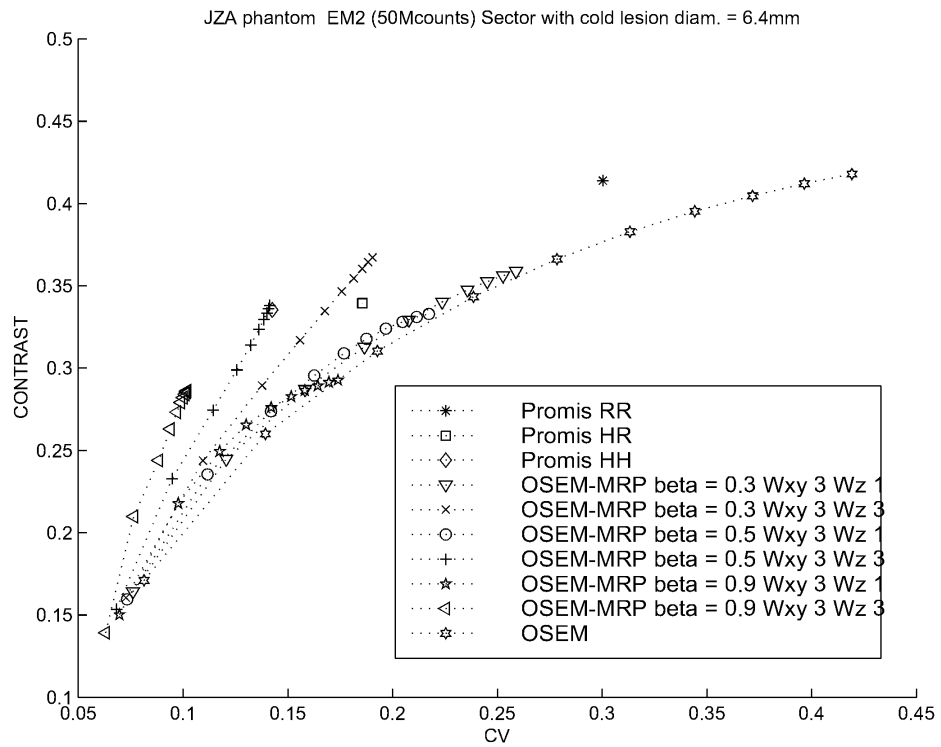
Figure 5.4-3: JZA phantom cold bar dimensions 6.4 mm. Contrast as a function of CV.
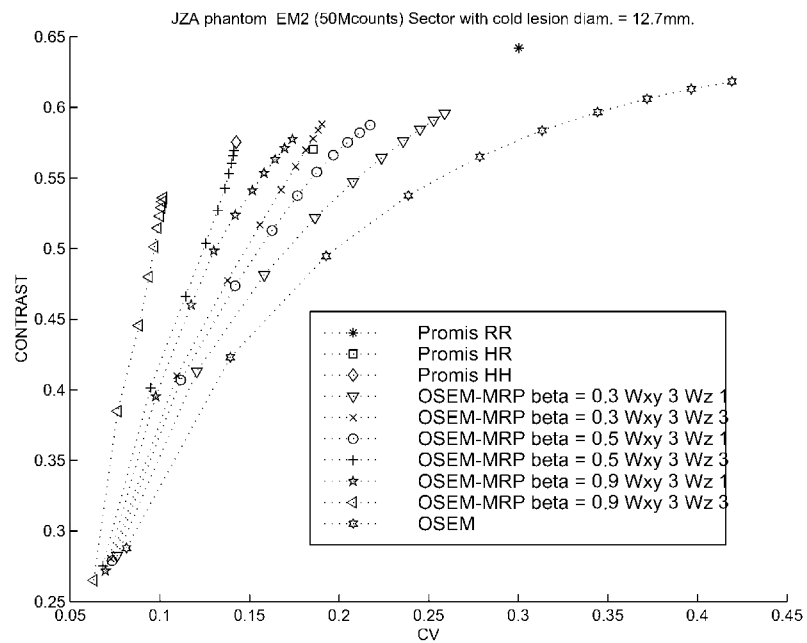

Figure 5.4-4: JZA phantom cold bar dimensions 12.7 mm. Contrast as a function of CV.

Figure 5.4-5 shows the reconstructed images of the JZA phantom for the high statistic(s) images (EM1). A better definition of the circular shape for the cold lesions in the OSEM-MRP images with respect to the Promis reconstructions is observable.
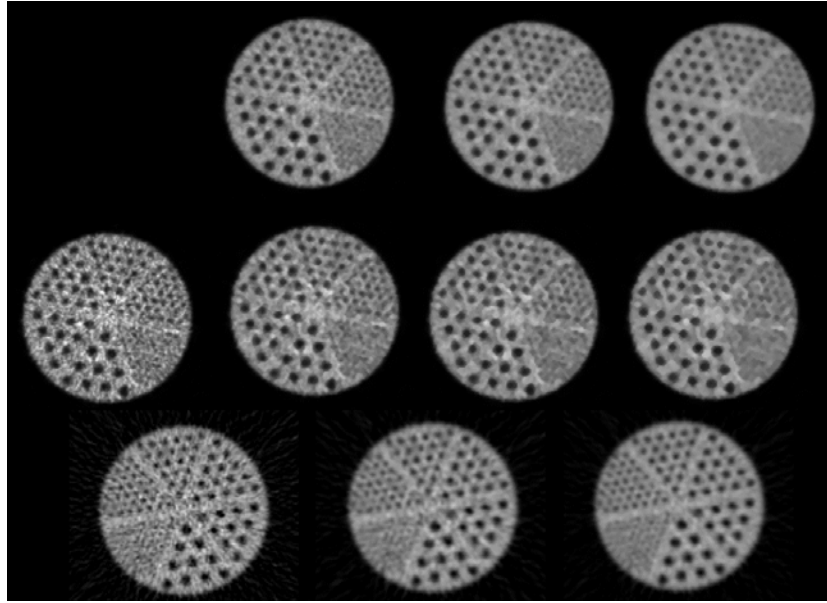
Figure 5.4-5: JZA phantom. The OSEM and OSEM-MRP images were obtained using 14 subsets, number of iteration=140
Top row (from left to right): OSEM-MRP3DM (β =0.3), OSEM-MRP3DM (β =0.5), OSEM-MRP3DM(β =0.9).
Middle row (from left to right): OSEM, OSEM-MRP2DM (β=0.3), OSEM-MRP2DM(β =0.5), OSEM-MRP2DM(β =0.9)
Bottom row (from left to right): PromisRR, PromisHR, PromisHH

5.4.3 HB Phantom

Figure 5.4-6 shows the ratio between the activity measured in the "grey " and "white" matter regions as a function of the coefficient of variation for the "grey" (/ "white") matter. As the Hoffman brain phantom has been built to produce an activity ratio of 4:1 (of activity) between grey and white matter the most accurate ratio was obtained with OSEM and OSEM-MRP2DM. OSEM-MRP3DM for β =0.3 and 0.5 performed as well as PromisRR and PromisHR.
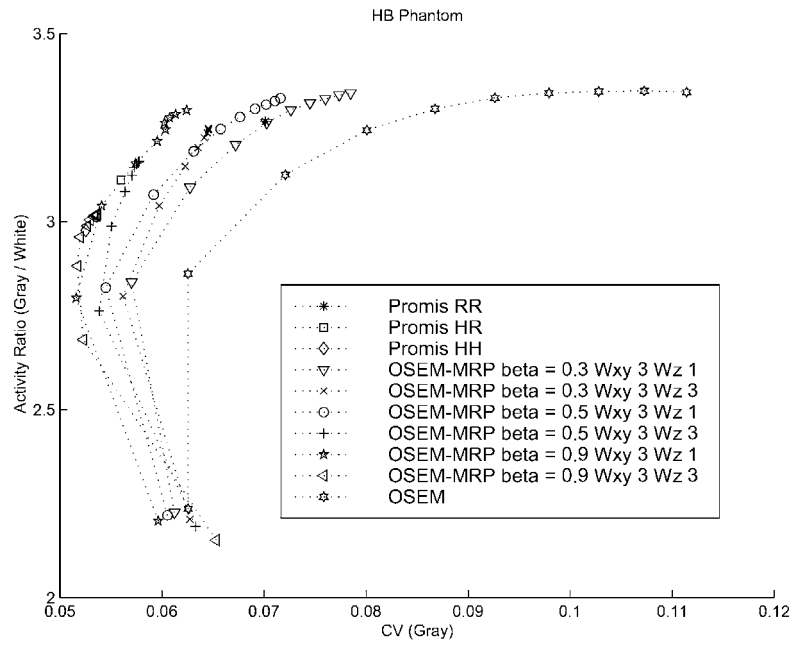
Figure 5.4-6: HB phantom. Activity ratio as a function of the CV (calculated for grey matter)

Figure 5.4-7 shows representative slices of the Hoffman Brain phantom reconstructed with different algorithms and parameter configurations. The noise suppression is clearly evident in the OSEM-MRP3DM images without loss of resolution.
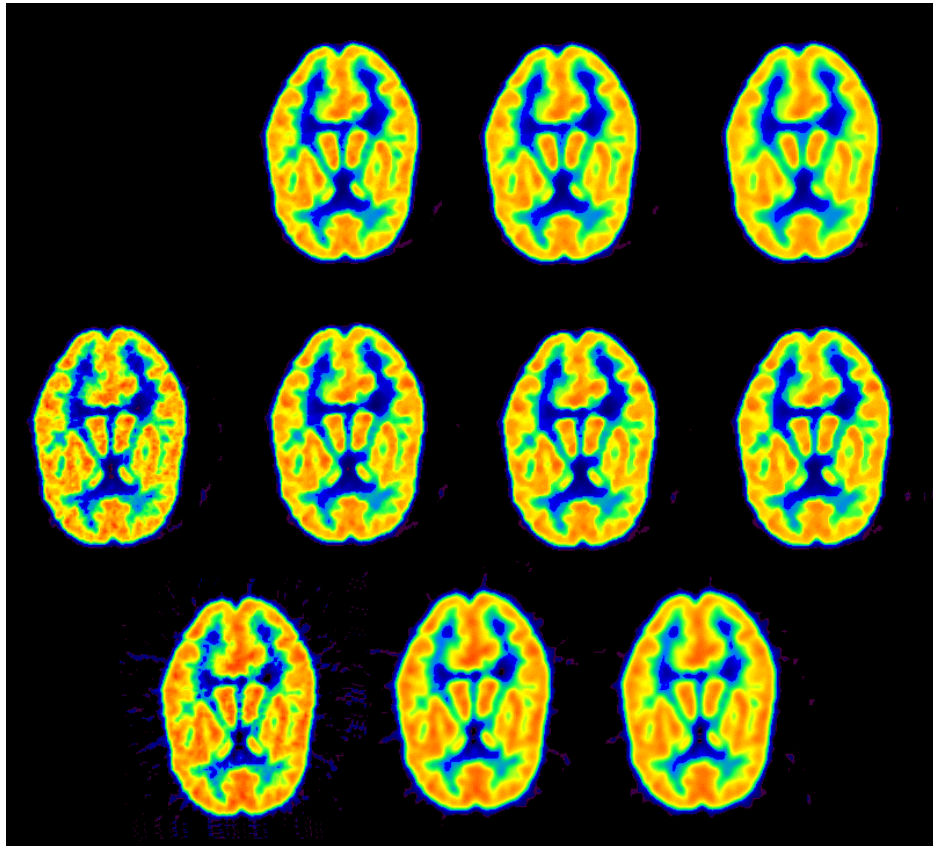

Figure 5.4-7: HB phantom - The OSEM and OSEM-MRP images were obtained using 14 subsets, number of iterations =140. See Figure 5.4-5 for the order of the images.

5.4.4 ST phantom

Figure 5.4-8 shows the ratio between the activity measured in the "putamen" and in the background ROIs as a function of the CV calculated on the background. The true value of the ratio is 3.84. OSEM achieves the highest and most precise activity ratio but on the other hand the noise level is even higher than with PromisRR. All OSEM-MRP configurations show a higher ratio of activity than PromisHH and PromisHR and have a clear tendency to converge to a stable value. Similar results were obtained for the "caudate" structure.
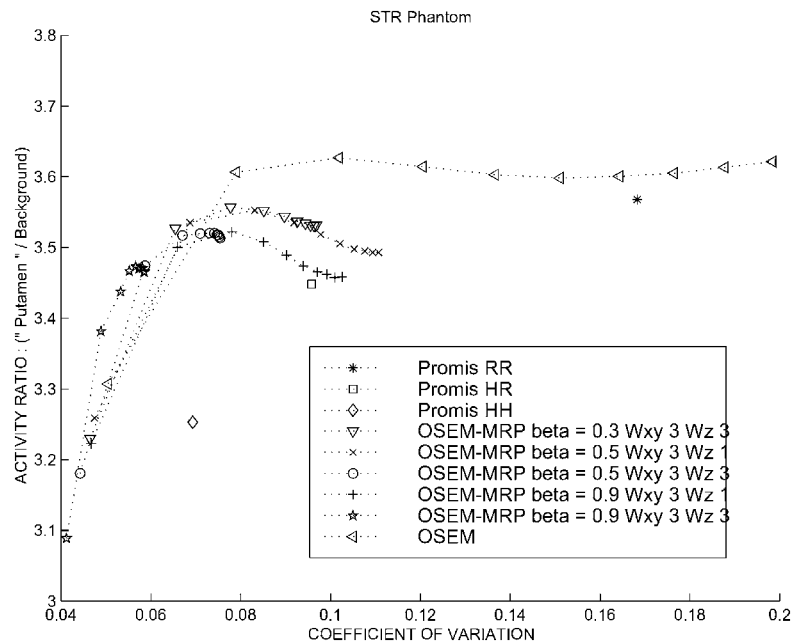

Figure 5.4-8: ST phantom. Activity ratio as a function of the CV (calculated for the background)

Figure 5.4-9 shows the images of the ST phantom reconstructed with different algorithms and parameter(s) configurations. The noise suppression is clearly evident in the OSEM-MRP images and without loss in resolution, particularly when 3DM is used in the reconstruction.
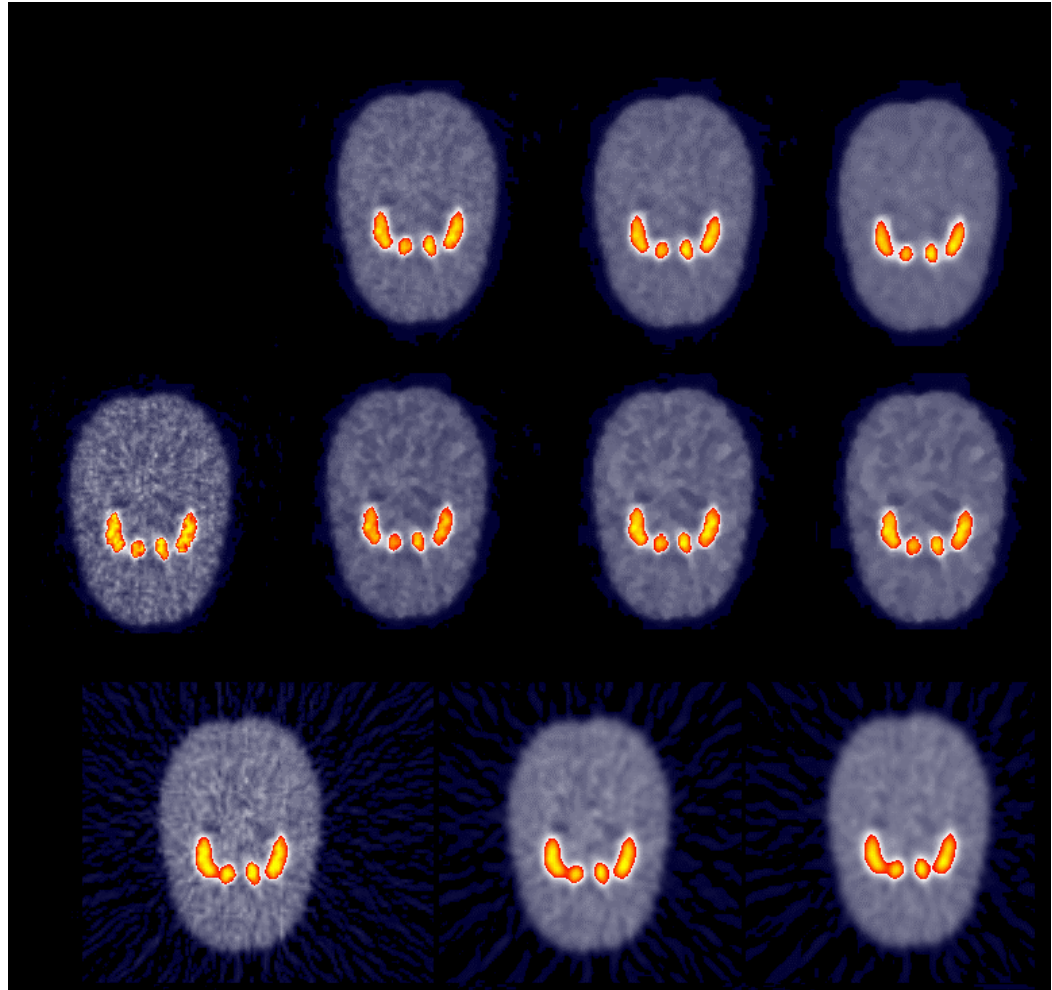
Figure 5.4-9: ST Phantom - The OSEM and OSEM-MRP images were obtained using 14 subsets, number of iterations =140. See Figure 5.4-5 for the order of the images.

5.5 Discussion and Conclusions

We have implemented and evaluated a 3D OSEM-MRP algorithm for 3D PET brain studies. The algorithm was evaluated using experimental phantoms simulating the shape and dimensions of brain structures. Pre-corrected data were used as input to the reconstruction algorithms. The results have shown that the 3D OSEM-MRP algorithm confirms the good properties already found with 2D data-sets in terms of noise reduction, resolution and convergence. In all the experimental situations, 3D OSEM-MRP is shown: 1) to converge to a stable solution, 2) to be quantitatively accurate, 3) to be very effective in noise reduction, particularly for low statistics data, 4) to maintain "good" spatial resolution. These properties have been shown both with high and low statistics data, proving the robustness of the algorithm in different conditions of activity ratio and activity distribution.

Compared with the 3D OSEM and PROMIS algorithms, 3D OSEM-MRP provide better or comparable results depending on the configuration parameters used for the reconstruction of the images. It would be possible to optimise the parameters of the OSEM-MRP algorithm for a specific task.

6. ART-type algorithms

This section discusses the evaluation of the variable-Block Algebraic Reconstruction Technique, variable in the sense that the block structure, their organisation and their characteristics change with iteration number. The material from this section is taken from [Sad00].

We performed 'multi-level' image reconstructions by changing the structures of the blocks during the iterations. In particular, we increased the block size, taking more and more data into account during successive iterations. This process is used jointly with inter-iteration Metz filtering.

6.1 Data

The evaluations presented here were done on the acquisition (200M counts) of the Jaszczak phantom on the GE Advance phantom mentioned in the previous sections. Contrast ratios quoted in this section are for the cold regions of diameter 0.79cm.
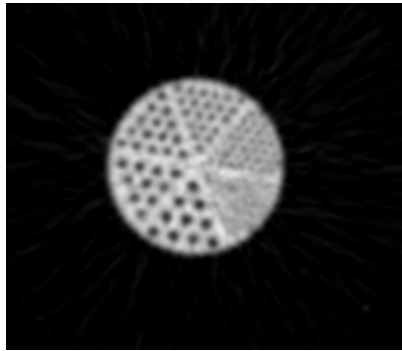

Figure 6.1-1: Sample reconstruction (10 iterations) of the Jaszczak phantom with Block-ART. 21 subsets were used, with Metz filtering after every full iteration. The plane is near the centre of the scanner.

6.2 Reconstruction set-up

Dynamic block composition

We have studied the behaviour of different configuration of blocks, from the most advantageous as regards parallelism - that is where one block represents one or two whole segments - to configurations which are the least adapted to parallelism, where the block represents one projection only. The configurations included not only static blocks but also dynamic ones (variable), which change throughout the iterations.

 Most calculations in this study used blocks such that the symmetries in the projection matrix could be exploited as much as possible. We also tried to distribute the blocks evenly over the available processors, to minimise calculation time. Nevertheless, some calculations were performed with 'inefficient' block configurations to see if better results could be obtained.

Filtering

The reconstructions were performed without filtering or with a Metz filter of power 1 XF=.05, ZF= .08 (see section 4.1) with up to 10 iterations. We considered two approaches for the filtering: either after each update of the image by a block (inter-block filtering) or after every full iteration (inter-iteration filtering).

6.3 Results

Block configuration

We found that too small blocks (consisting of only a few measured LORs) resulted in poorer image quality, compared to using the same size of blocks as discussed in the evaluation of OSEM (i.e. block sizes of about 1/20 the total data size). Making the blocks even larger did not give any improvements on the visual image quality and only small improvements on the FOMs (see Figure 6.3-1-Figure 6.3-2). Taking into account the increased CPU time per iteration, this shows that having ~20 subsets is the optimal choice (for this scanner).
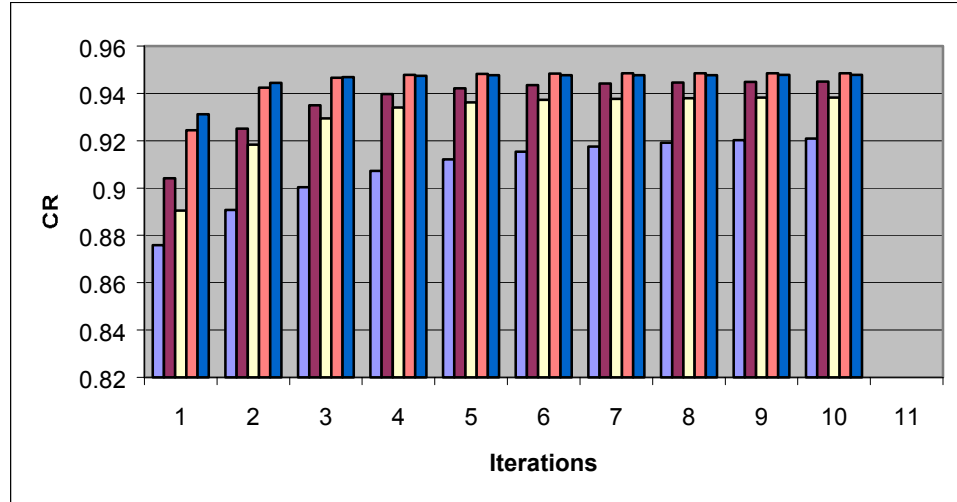

Figure 6.3-1: Contrast recovery for different block structures. Block configurations are as follows: (1) all segments, 1 view; 2 segments, all views; (3) 1 segment, 1 view;(4) all segments, 21 views (no symmetry in views); (4) all segments, 84 views (symmetry in views)
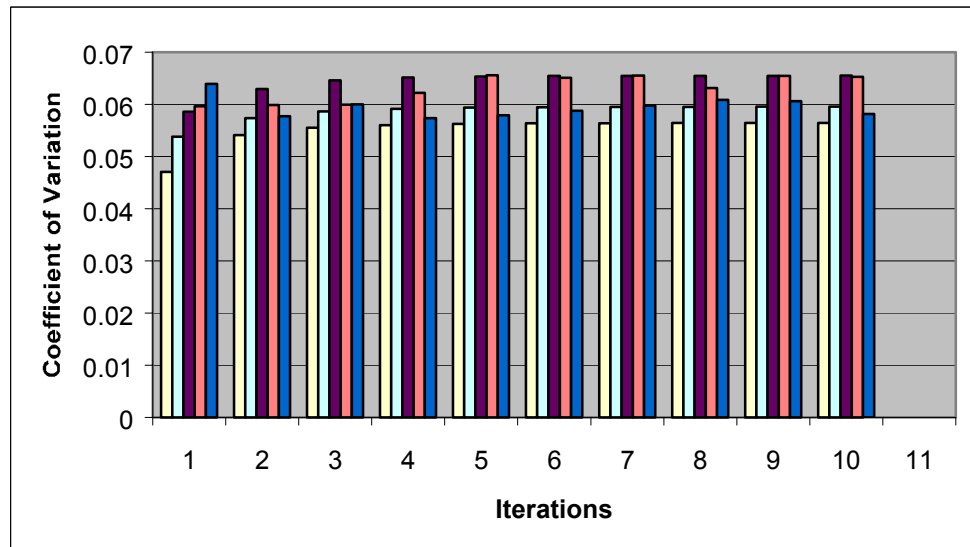

Figure 6.3-2: Coefficient of variation for different block structures. See previous figure for block configuration.

Order of blocks

Two different orders were used: the block sequential presentation order and a random order. However, the two FOMs under study did not depend appreciably on the choice of order. This was the case both with and without filtering

Filtering

The inter-block filtering scheme resulted in very slow convergence in the outer planes. Also, at initial iterations the end-planes showed too low intensity. This is probably due to the fact that all blocks contain information on the middle planes, while only few of them modify the end planes. The inter-block iteration mean there is filtering after every update, effectively suppressing changes in the images. As the changes are smaller for the end planes, this means they will show slower convergence. This was not a problem with the inter-iteration filtering scheme.

This behaviour manifested itself in both FOMs: in the outer planes, stable CR and CV where achieved at much later iteration numbers for the inter-block filtering compared to inter-iteration filtering. However, in the middle planes, convergence speed was similar for both filtering schemes (see Figure 6.3-3).

Finally, with the settings of the filter we tried, the inter-block scheme resulted in over-smoothing. This is illustrated in the CR values in Figure 6.3-3.
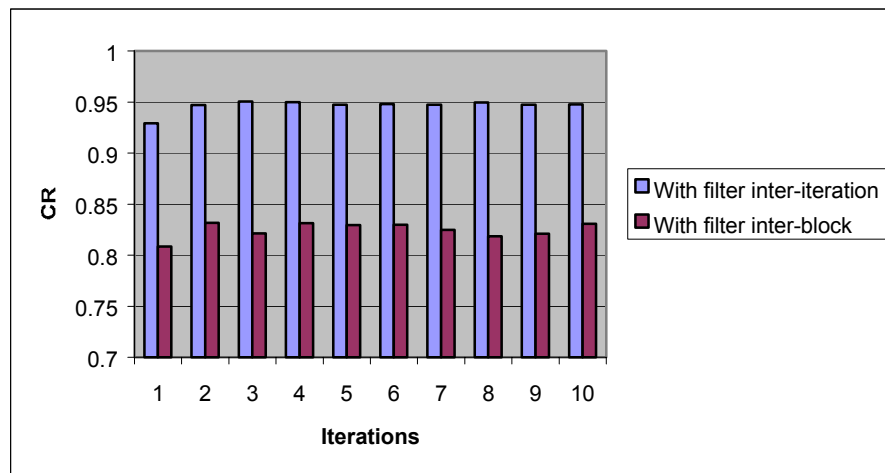

Figure 6.3-3: Influence of inter-block or inter-iteration filtering on Contrast Recovery in the middle plane. Block configuration is as in (4) in Figure 6.3-1.

6.4 Conclusion

The results of the image evaluation, by using different FOMs, show clearly the importance of the choice of the structure of blocks used during the reconstruction. We find that about 20 blocks is a good compromise between quality and reconstruction speed. We clearly illustrated that for Block ART, inter-iteration filtering is superior to inter-block filtering. The question of how to choose the 'variable blocks' to achieve optimal results needs further investigation. However, as we find that results are not very dependent on block size (as long as the block does updates the whole image), we suggest to do an initial iteration with only the direct planes of the sinogram data (segment 0). This effectively initialises the 3D-ART algorithm with a good first estimate.

7. Conclusions

In general, OSEM results in more noisy images than OSMD and OSCB, but the noise can be considerably reduced by filtering without appreciably impairing contrast. Application of the MRP leads to convergence of OSEM to a stable solution within a reasonable number of iterations but the noise properties relative to PROMIS are found to depend on the parameters chosen. The preliminary analysis of Block ART seems to indicate that with a good choice of blocks, convergence is very fast. Moreover, when applying inter-

iteration filtering, the uniformity of the image stays good while obtaining high contrast ratios.

Iterative methods can give better contrast and signal-to-noise properties than PROMIS but judicious choice of filtering and prior information needs to be made and depends on the tracer distribution and noise level of the data. This is true for both analytic and iterative algorithms.

8. References

[Ale97] Alenius S, Ruotsalainen U, 1997, Bayesian image reconstruction for emission tomography based on median root prior *Eur. J. Nucl. Med* 24, No. 3, 258-265.

[Ale98] Alenius S, Ruotsalainen U, Astola J, Using local median as the location of the prior distribution in iterative emission tomography image reconstruction, *IEEE Trans. on Nucl. Sc.*, 45:3097-3104.

[Bet00] Bettinardi V, Pagani E, Alenius S, Teras M, Gilardi M C, Labbé C, Jacobson M, Thielemans K, Sadki M, Implementation and evaluation of a 3D Ordered Subsets Expectation Maximization and Median Root Prior (3D-OSEM-MRP) reconstruction algorithm for 3D PET studies. In preparation.

[Dau99] Daube-Witherspoon M E, Karp J S 1999 Measurement of Image Quality in 3D PET. Proceedings of the 1999 International Meeting on Fully Three-Dimensional Image Reconstruction in Radiology and Nuclear Medicine pp. 69-72

[GEMS] General Electric Medical Systems homepage http://www.gems.com

[Hud94] Hudson H M and Larkin R S 1994 Accelerated image reconstruction using ordered subsets of projection data. *IEEE Trans. Med. Imaging* 13 No. 4, pp. 601-609.

[Jac00] Jacobson M, Levkovitz R, Ben-Tal A, Thielemans K, Spinks T, Belluzzo D, Pagani E, Bettinardi V, Gilardi M C, Zverovich A, Mitra G, Enhanced 3D PET OSEM Reconstruction Using Inter-Update Metz Filtering, accepted for publication in *Phys. Med. Biol.*

[Kin89] Kinahan P.E and Rogers J.G. 1989 Analytic 3D image reconstruction using all detected events *IEEE Trans. Nucl. Sci.* 36 pp. 964-968.

[Lab98] Labbé C, Thielemans K, Zaidi H., Morel C 1998 An object oriented library incorporating efficient projection/back projection operators for volume reconstruction in 3D PET. Proceedings of the 1999 International Meeting on Fully Three-Dimensional Image Reconstruction in Radiology and Nuclear Medicine, pp. 137-140. Available at http://www.brunel.ac.uk/~masrppet.

[Mar99] Margalit T, Gordon T, Jacobson M, Ben-Tal A, Nemirovski A, Levkovitz R, "The Ordered Sets Mirror Descent and Conjugate Barrier optimization algorithms adapted to the 3D PET reconstruction problem", submitted to *IEEE Trans. Med. Im.*

[NEMA] Performance Measurements of Positron Emission Tomographs. NEMA Standards Publication NU 2-1994.

[Nuy99] Nuyts J., Dupont P, Stroobants S, Maes A, Mortelmans L, and Suetens P. 1999 Evaluation of maximum likelihood based attenuation correction in positron emission tomography. *IEEE Trans. Nucl. Sc.* 46 No. 4 pt. 2 pp.1136-41.

[Sad00] Sadki M, Mitra G, Spinks T, Thielemans K: Parallel implementation and evaluation of Variable-Block-ART algorithms for positron emission tomography. To be submitted

[She82] Shepp L A and Vardi Y 1982 Maximum likelihood reconstruction for emission tomography. *IEEE Trans. Med. Imaging* **1** pp.113-122.

[Sli98] Slijpen E T P, Beekman F J 1998, Comparison of post-filtering and filtering between iterations for SPECT reconstruction, IEEE Nuclear Science Symposium.and Medical Imaging Conference **2** pp. 1363-6.

[Thi99] Thielemans K, Jacobson M W, and Belluzzo D 1999 On various approximations for the projectors in iterative reconstruction algorithms for 3D PET. Proceedings of the 1999 International Meeting on Fully Three-Dimensional Image Reconstruction in Radiology and Nuclear Medicine, pp. 232-235. Available at http://www.brunel.ac.uk/~masrppet

[Thi00] Thielemans K and Jacobson M, On various approximations for the projectors in 3D PET reconstruction. To be submitted.

[Tow93] Townsend D W, Wensveen M, Byars L G, Geissbuhler A, Tochon-Danguy H J, Christin A, Defrise M, Bailey D L, Grootoonk S, Donath A 1993 A rotating PET scanner using BGO block detectors: design, performance, and applications. *J. Nucl. Med.* **34** pp. 1367-1376.

[Var85] Vardi Y, Shepp L A, and Kaufman L 1985 A statistical model for positron emission tomography. *Journal of the American Statistical Association* **80** No. 389, pp.8-20.